Regional Features of the 20-30 Day Periodic Behavior in the Southern Hemisphere Summer Circulation

Zhaoyu Liu[1] and Lei Wang[1]

[1]Purdue University

May 2, 2023

Abstract

The Southern Hemispheric (SH) storm tracks exhibit a robust intraseasonal periodicity of 20-30 days as the leading mode of zonal-mean eddy kinetic energy. To what extent this hemispheric-scale mode of variability translates to smaller scales remains debated. This work studies the regional features of SH storm tracks through the filtered variance of local finite-amplitude wave activity. While the synoptic variance is zonally elongated over the storm track, we find a strong enhancement of intraseasonal variability within the South Pacific with a minimum strength of the storm track. This enhanced region is marked with 20-30 day periodic behavior of local wave activity and precipitation and is driven by enhanced variability of low-level eddy heat flux on the same timescale. The local nature of 20-30 day periodicity offers a potential source of intraseasonal predictability for weather analysts and forecasters.

Regional Features of the 20-30 Day Periodic Behavior in the Southern Hemisphere Summer Circulation

Zhaoyu Liu[1], Lei Wang[1]

[1]Department of Earth, Atmospheric, and Planetary Sciences, Purdue University

Key Points:

- The hemispheric 20-30 day periodicity in the austral summer has a strong localization in local wave activity and precipitation.
- Strong enhancement of intraseasonal variability and local periodic behavior is identified within the South Pacific.
- The local nature of 20-30 day periodicity offers a potential source of intraseasonal predictability for weather analysts and forecasters.

Corresponding author: Lei Wang, `leiwang@purdue.edu`

Abstract

The Southern Hemispheric (SH) storm tracks exhibit a robust intraseasonal periodicity of 20-30 days as the leading mode of zonal-mean eddy kinetic energy. To what extent this hemispheric-scale mode of variability translates to smaller scales remains debated. This work studies the regional features of SH storm tracks through the filtered variance of local finite-amplitude wave activity. While the synoptic variance is zonally elongated over the storm track, we find a strong enhancement of intraseasonal variability within the South Pacific with a minimum strength of the storm track. This enhanced region is marked with 20-30 day periodic behavior of local wave activity and precipitation and is driven by enhanced variability of low-level eddy heat flux on the same timescale. The local nature of 20-30 day periodicity offers a potential source of intraseasonal predictability for weather analysts and forecasters.

Plain Language Summary

Storm activities in Southern Hemisphere (SH) midlatitudes are characterized by 20-30 day periodic behavior, representing a hemispheric-scale pulsing of zonal-mean extratropical eddy activity. This phenomenon has been termed the Baroclinic Annular Mode (BAM) defined as the leading EOF mode of the zonal-mean eddy kinetic energy. If this large-scale mode were to have a strong local nature, such periodic behavior in subseasonal-to-seasonal time scale would have important implications for understanding and predicting the medium-range weather system, especially for extreme events. However, to what extent we can identify regional features of such hemispheric-scale mode of variability remains unclear.

We demonstrate the regional feature of this periodic variability by showing the variance of local wave activity in different time scales. We find that the variability in a shorter weather time scale (2-7 days) exhibits a largely zonally-symmetric structure, but the variability in the intraseasonal time scale exhibits a strong localization concentrated in the South Pacific. We further assess the distribution of periodicity within the intraseasonal variability and find that the 20-30 day periodicity is also localized within South Pacific. The local nature of this 20-30 day periodicity indicates the potential utility of the BAM for weather analysts and forecasters.

1 Introduction

High-quality societal applications for decision-makers for optimizing resource management and preventing disaster require accurate sub-seasonal to seasonal (S2S, intraseasonal) predictions, because high-impact extreme weather events, such as long-lasting heatwaves and extreme cold spells, often occur on this timescale. Recent research has identified multiple sources of S2S predictability, such as the Madden-Julian oscillation (MJO), the basic state of the ENSO, soil moisture, tropical-extratropical teleconnections, etc (see the review in (Vitart et al., 2017)). However, nearly all of these sources are outside of the midlatitude internal dynamics. This is due to the conventional understanding that the large-scale midlatitude variability is typically consistent with Gaussian red noise rather than periodic behaviors (Feldstein, 2000; Lorenz & Hartmann, 2001). As a 'null hypothesis,' intraseasonal variability can be considered as a response to stochastic forcing by higher-frequency synoptic system's disturbances (Leith, 1973; Hasselmann, 1976; Green, 1977). Assuming synoptic disturbances as Gaussian white noise forcing F_t, this 'null hypothesis' suggests the time series of intraseasonal variability x_t as a Gaussian red noise process $x_t = \alpha x_{t-1} + F_t$, where α is a positive constant defining the e-folding timescale of the intraseasonal variability. Hence, no unique source of predictability on regional scales has been identified within the midlatitude atmosphere beyond the synoptic weather range.

Baroclinic Annular Mode (BAM), however, a recently discovered large-scale midlatitude variability over the SH, is characterized by a robust intraseasonal periodicity about 20-30 day (Thompson & Barnes, 2014; Thompson & Woodworth, 2014). BAM is defined by the leading empirical orthogonal function (EOF) of the zonal-mean eddy kinetic energy (EKE), representing the intraseasonal oscillation of eddy activity on a hemispheric scale. If such periodic nature were to translate to smaller scales at certain regions, it could serve as a new source of S2S predictability. In a regional scale study of BAM, Thompson et al. (2017) find that the periodicity in the upper troposphere eddy kinetic energy is not apparent at a fixed location. As the averaging windows reduce from the entire global circle to 30-degree wide regions, the power spectra reduce from a robust quasi-periodic shape to a red noise without any major enhancement of the variance on the 20-30 day frequency range. The discovery of the lack of local periodicity for regions smaller than 30 degrees is explained through a conceptual model featuring out-of-phase anomalies between the upper and lower troposphere. A similar finding was also confirmed in Xue et al. (2021), that the domain should be wide enough to accommodate a wave packet so that the intraseasonal periodicity can be identified. Therefore, as the averaging domain size reduces to smaller scales, periodic behavior at a fixed region is not expected, which is consistent with the above 'null hypothesis.' To what extent such a leading mode of variability is translated to regional scale intraseasonal variability - and thus modulating serial clustering of extreme weather events - remains an open question.

To address this question, we will adopt a filtered variance approach, which has been well-developed to identify the geographic distributions of the storm tracks (Blackmon et al., 1977). Typically, a scalar quantity combining multiple information is preferred, such as the 500 hPa geopotential height field (Z500), which is related to both the wind and temperature. Blackmon et al. (1977) developed this filtered variance framework using the Northern Hemisphere (NH) Z500, with the spectral domains separated into synoptic and intraseasonal bands, respectively (also see Blackmon et al. (1984)). Through a similar filtered variance analysis, Trenberth (1981, 1991) studied the SH circulation within synoptic time scales and found that the SH storm tracks exhibit strong zonal symmetry along with a maximum located at the Southern Indian Ocean and a minimum at the South Pacific. Kidson (1991) found a zonal-symmetric pattern for the intraseasonal variability in the SH (see also Hartmann (2015)). Therefore, we aim to make progress on deepening the understanding of the regional features of the intraseasonal variability - a less explored territory. Specifically, we ask: are these regions with enhanced intraseasonal variance mainly characterized by a Gaussian red-noise spectrum as expected from the 'null hypothesis,' or have certain quasi-periodic behaviors that may be connected with the hemispheric-scale 20-30 day periodic mode of variability?

To answer this question, we start with the surface precipitation analysis, a directly measured quantity as a surrogate for the local behavior of storm activities. Then we will quantify the regional variability pattern by applying the filtered variance approach (Blackmon et al., 1977) to key representative variables, including Z500, EKE, and a newly developed quantity local wave activity (LWA), as well as the low-level eddy heat flux that drives LWA tendency. This work focuses on Austral summer season (DJF) since the periodic behavior is much more significant in austral summer than other seasons (Wang & Nakamura, 2015). Comparisons to the Northern Hemisphere and with different seasons will be addressed in follow-up studies. The paper is organized as follows. In Section 2, we introduce data and key methodologies such as LWA and filtered variance framework. In Section 3, we first discuss the regional features of surface precipitation and then demonstrate the synoptic and intraseasonal variability patterns of different variables associated with spectral analysis. Section 4 concludes with a summary.

2 Data and Method

We use ECMWF-Interim reanalysis products, including zonal and meridional velocities, air temperature, and geopotential height, with a horizontal resolution $1.25° \times 1.25°$ and daily resolution from 1979 to 2018. Additionally, the daily precipitation is obtained from the Advanced Microwave Scanning Radiometer(AMSR) -E from 2003 to 2010 processed by a three-day moving average. AMSR-E measures the surface rain rate covering from 70°N-70°S.

The filtered variability approach is based on the standard deviation in the 2-7 day band for synoptic analysis and the 10-45 day band for intraseasonal analysis. The temporal filter is based on Fast Fourier Transform (FFT) with Hanning window from 1 December to 28 February between 1979 and 2018. The framework is applied to Z500, EKE, LWA, and 850hPa eddy heat flux, respectively. EKE is defined as $((u^*)^2+(v^*)^2)/2$ and is averaged with density weighting along the vertical column. 850hPa eddy heat flux is defined as v^*T^*, where the asterisks represent the departures from the zonal mean.

Unlike EKE, local finite-amplitude wave activity emphasizes on coherent meandering of the contours of a quasi-conserved quantity. Conserving flow circulation through Kelvin's circulation theorem, the area bounded by the reference quantity contour is the same as the one bounded by the latitude circle. Finite-amplitude wave activity (FAWA, see N. Nakamura and Zhu (2010)) focuses on the total displacement over the entire longitudes, while LWA (see Huang and Nakamura (2016), Chen et al. (2015)) measures the displacement for each longitude, so that a full longitude-latitude pattern of wave activity can be quantified. For example, the field of Z500 can be used to define the local wave activity (Chen et al., 2015):

$$A_{z500}(\phi_e, \lambda, t) = \frac{a}{cos\phi_e}\left(\int_{z'\geq 0, \phi\leq\phi_e, \lambda=const} z' cos\phi d\phi - \int_{z'\leq 0, \phi\geq\phi_e, \lambda=const} z' cos\phi d\phi\right), \quad (1)$$

where a is the earth radius, ϕ, λ, represents the latitude and longitude respectively, $z' = z - Z(\phi_e)$ is the deviation from the reference Z500 contour $Z(\phi_e)$ at its equivalent latitude ϕ_e. The relation between $Z(\phi_e)$ and ϕ_e is connected by the same bounded area $\phi_e(Z) = arcsin[1 - \frac{S(Z)}{2\pi a^2}]$.

A quasi-geostrophic potential vorticity (QGPV) -based LWA allows one to quantify the role of eddy forcing. Local wave activity at each pseudo-height level can be assessed independently, and the density-weighted vertically averaged value is used to represent the barotropic wave activity. See supplementary material for more details.

3 Results

We start with analyzing the temporal and spatial features of precipitation, since surface rain rate is a directly measured quantity by space-based meteorological satellites, and is highly correlated with the variability of storm activity. Thompson and Barnes (2014) found that the mid-latitude mean precipitation can also exhibit a significant intraseasonal periodicity around 20-30 days as a key feature of BAM. Is there any localization of such periodic behavior in the precipitation?

To illustrate the regional feature, we calculated the power spectra of surface rain rate retrieved from AMSR-E in four separated regions as shown in Figure 1c: 0°-90°E, 90°E-180°, 180°-90°W, 90°W-0°, all of which are averaged between 40°S-50°S, and we find that the most significant 20-30 day periodicity is located at the South Pacific (180°-90°W with 95% confidence level), while spectra features in other three regions are mainly characterized by enhanced synoptic variability (0°-180°E) or similar to a red-noise (90°W-0°). Thus, there is a localization of the surface rain rate's 20-30 day periodic behavior. Is this localization of rain rate periodicity a coincidence? Or it implies a strong local-

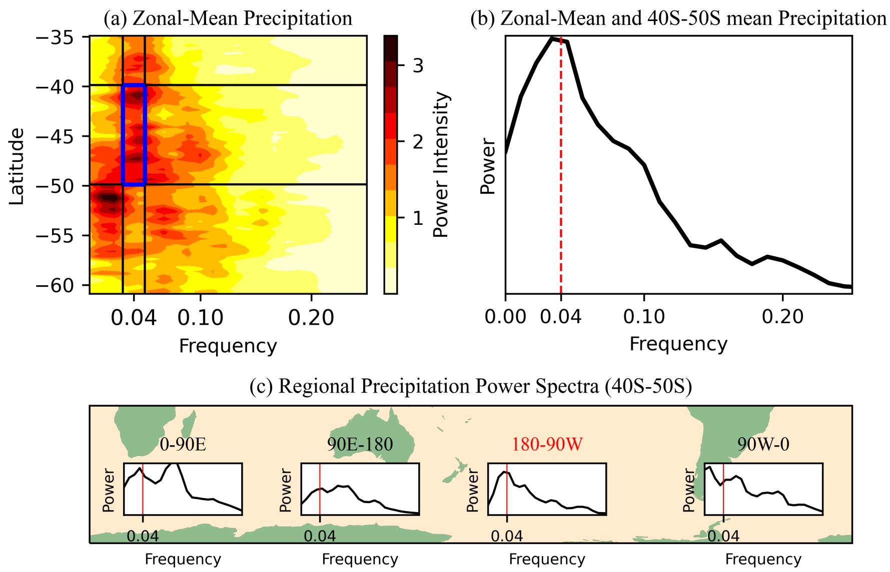

Figure 1: Power spectra of surface precipitation in austral summer(DJF) from 2002-2010 for (a)zonal-mean, (b)zonal-mean and averaged between 40°S-50°S, (c)regional mean of 0°-90°E, 90°E-180°, 180°-90°W, 90°W-0°, all of which averaged between 40°S-50°S.

ization of the 20-30 day periodic behavior for the underlying large-scale atmospheric circulation?

We adopt the filtered variance approach of Blackmon et al. (1977) to quantify the regional features of synoptic and intraseasonal variability, respectively. The variability of Z500 exhibits a more zonally symmetric regional pattern within both synoptic and intraseasonal timescales as consistent with the previous work (see Supplementary Figure S1). Centered around 50°S, the synoptic variance is strongest in the South Indian Ocean, while the maximum of intraseasonal variance is zonally elongated over much of the South Pacific. The zonal-mean Z500 field does not show any periodic behavior in the intraseasonal timescales (see Supplementary Figure S2), thus we would not expect any local periodic behavior in the Z500 field.

As the variable central to the BAM definition, zonal-mean EKE is characterized by a robust periodic behavior (Thompson & Woodworth, 2014). However, as Thompson et al. (2017) discovered, the periodicity in EKE is not apparent at a fixed location, and we find consistent results that the regional variability is much weaker in the intraseasonal band at pixel(i.e., grid point) level (see Supplementary Figure S3). Instead, a two-branch structure is observed in the intraseasonal variance pattern of EKE, and can be attributed to the intense wave-breaking processes at the South Pacific that generate intense local values of zonal and meridional velocities, since qualitatively speaking, EKE reaches maximum where the circulation contours are the densest. The two-branch structure belongs to the same storm activity region - as the below LWA analysis would illustrate more clearly.

Therefore, an accurate diagnostic approach for eddy activity that can illustrate both spatial and temporal features is required to study our key question. As a comparison with Z500 or EKE, the local finite-amplitude wave activity (LWA) provides a more objective

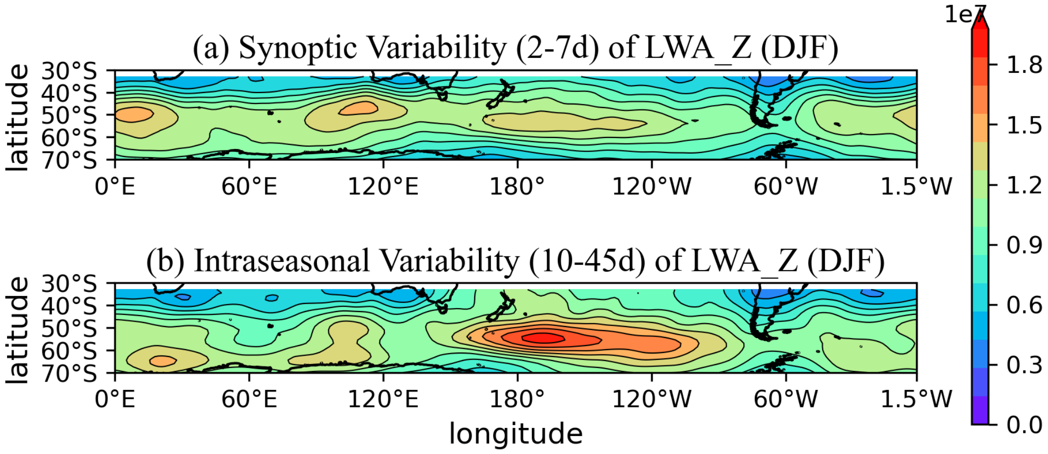

Figure 2: Bandpass-filtered variance converted to standard deviation for Z500_based LWA (LWA_Z) in austral summer(DJF): (a)synoptic variability(2-7 days), and (b)intraseasonal variability(10-45 days). The shading represents values between $0m^2$ and $1.9 \times 10^7 m^2$.

approach for the diagnostic of eddy activity. QGPV-based LWA is a conserved quantity and driven by eddy flux terms - each bearing clear physical interpretations, directly representing the pseudo-momentum carried by eddy. Z500-based LWA shares many features of the QGPV-based LWA, and it is more straightforward to calculate. Regarding the spatial feature, LWA can capture the breaking waves as part of an underlying coherent pattern (see the comparison between LWA and EKE in Huang and Nakamura (2017)). For example, for a large-scale dipole structure, the maximum value of LWA locates only at the center of the overturning contours of PV (or Z500). In contrast, the maximum values of EKE are found at two distinct places - the edge of the upper high-pressure system and the edge of the lower low-pressure system. Regarding the temporal feature, Wang and Nakamura (2015) confirmed that FAWA also exhibits a robust 20-30 day periodicity, consistent with features of BAM defined by the EOF-based EKE framework. Since zonal-average of LWA naturally conforms to FAWA, LWA has the strength to pinpoint regional features more precisely, and to allow for a direct connection with the hemispheric-scale 20-30 day periodic behavior as defined by FAWA. Both the QGPV and Z500 fields can be used to calculate the LWA, with the former directly connected with the eddy fluxes terms and the latter more commonly available among climate model outputs. Our analysis confirms that both approaches yield qualitatively consistent results.

Figure 2 shows the synoptic and intraseasonal variability pattern of Z500-based LWA in austral summer. The synoptic variability still exhibits a zonally symmetric pattern, with the maximum variance concentrated in the Southeast (SE) Indian Ocean as well as in the SE Atlantic, and the minimum variance in the SE Pacific close to South America (also see Supplementary Figure S4 for QGPV-based LWA). This result is qualitatively consistent with the pattern shown by the filtered variance of the Z500 field, but further captures a more detailed and coherent structure clearly emphasizing the maximum region. Such intensified synoptic variability at the SE Indian Ocean and Atlantic can be largely attributed to the downstream development of baroclinic waves (Berbery & Vera, 1996), and therefore the largest synoptic variance is expected to occur closely downstream to the regions of maximum observed baroclinicity, which is located at the Southwest (SW) Indian Ocean and SW Atlantic (the sea surface temperature frontal zones, see H. Naka-

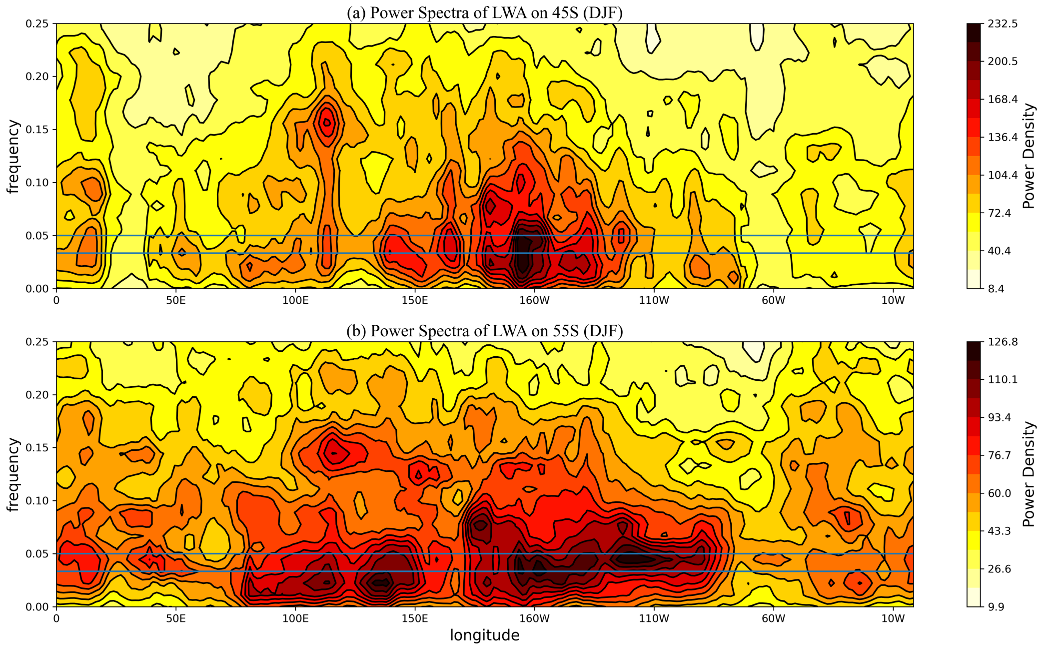

Figure 3: Power spectra of QGPV-based LWA as functions of longitude and frequency at two representative latitudes 45°S (upper panel) and 55°S (lower panel), respectively.

mura and Shimpo (2004)). The weakened synoptic signal at the South Pacific is associated with the decaying process of extratropical cyclones' lifecycles.

With an ability to capture larger-scale meandering, the filtered variance of Z500-based LWA captures the corresponding intraseasonal variability more efficiently than that of the Z500 and EKE field. As shown in Figure 2b, the intraseasonal variance of LWA is near twice its synoptic counterpart. Besides, the intraseasonal pattern is not as zonally-elongated as the synoptic variance or the pattern captured by Z500. In contrast, a strong local enhancement is found confined at the South Pacific, largely within 180°-150°W and 50°S-60°S. This region is right at the center between the two branches shown in the intraseasonal pattern of EKE (Supplementary Figure S3b), which demonstrates the advantage of LWA in capturing coherent patterns for large-scale eddies. Similarly, the filtered variance of QGPV-based LWA shows consistent results: a robust intensification of intraseasonal variability at the South Pacific is observed located within 180°-150°W (see Supplementary Figure S4b). Despite the minor difference that the QGPV-based LWA shows a more equatorward intraseasonal pattern, both types of the filtered variance of LWA show a consistent key region of intraseasonal variability of storm activities confined within the South Pacific.

With a region of enhanced intraseasonal variance pinned down, we next investigate whether the enhanced frequencies is related to the 20-30 day periodic mode. To zoom into the crucial latitudes where such periodicity is concentrated. Figure 3 shows the power spectra of QGPV-based LWA as the function of longitudes and frequencies at 45°S and 55°S, since Wang and Nakamura (2015) found that the 20-30 day periodic variability mainly dominates the midlatitudes from 40°S-60°S (also see Supplementary Figure S5). Within the intraseasonal domain, the 20-30 day periodicity (0.03-0.05 cpd, bounded by two blue

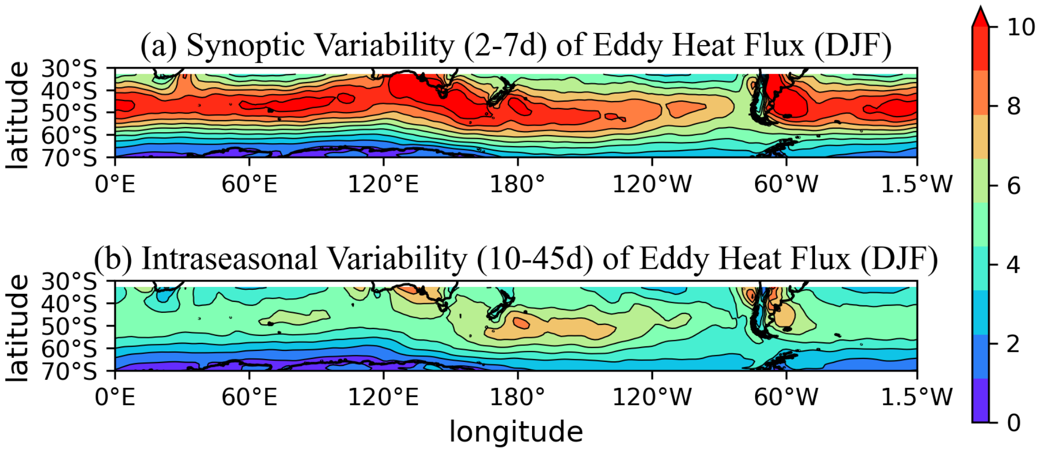

Figure 4: Bandpass-filtered variance converted to standard deviation for 850hPa eddy heat flux in austral summer(DJF): (a)synoptic variability(2-7 days), and (b)intraseasonal variability(10-45 days). The shading represents values between $0mK/s$ and $10mK/s$.

lines in Figure 3) exhibits a strong localization as hinted by the filtered variance approach. At 45°S for example, the strongest 20-30 day frequency band is largely confined between 180°-150°W, overlapping the region where the intrasesonal variance reaches its maximum (shown in Figure 2b). This regional feature of periodicity might slightly vary with different latitudes, for example the most significant 20-30 day periodicity at 55°S exhibits an elongated range covering 180°-100°W. By and large, all cross sections within midlatitudes demonstrate that the 20-30 day periodicity has a strong regional preference located at the South Pacific. A similar result can be observed if the LWA is meridionally averaged between 40°S-60°S (see Supplementary Figure S6), the 20-30 day periodicity is still strongly localized at the South Pacific, resembling the pattern at individual latitudes. Note that, in this case, the budget term of meridional eddy momentum flux is removed due to the meridional average, and therefore it can suggests that, the meridional eddy momentum flux plays a non-dominant role in the intraseasonal variability. The zonal wave flux convergence, as another important budget term of LWA, will not directly impact LWA's intraseasonal variability neither, as the zonal wave flux convergence primarily populate the synoptic variability of wave activity (Huang & Nakamura, 2017). The cross-section of power spectra for Z500-based LWA shows similar results to the QGPV-based LWA, whereas that for EKE does not show robust 20-30 day periodicity (see Supplementary Figure S7 and S8).

What would be a key factor that drives such locally confined intraseasonal variability including the 20-30 day periodicity? Wang and Nakamura (2015, 2016) find that eddy forcing due to the low-level eddy heat flux drives the 20-30 day periodicity in zonal-mean of LWA (i.e., FAWA). A local enhanced variance of eddy heat flux should be expected if this can also translate into regional scales. Figure 4 confirmed this expectation by showing that the intraseasonal variance of 850hPa eddy heat flux is also localized between 180°-150°W, largely overlapping the region where the intraseasonal variance of LWA is strongly enhanced, as shown in Figures 2 and 3. The cross-section power spectra of 850 hPa eddy heat flux further indicates that the low-level eddy heat flux also exhibits enhanced 20-30 day periodicity at fixed locations, largely confined within the South Pacific as well (see Supplementary Figure S9). This locally enhanced intraseasonal variability of 850hPa eddy heat flux is marked with a strong r.m.s. eddy streamfunction as a surrogate of eddy diffusivity for estimating the horizontal eddy heat flux (Kushner &

Held, 1998; Held, 1999). Strong thermal damping over this area reduces linear baroclinic eddy growth rates (Swanson & Pierrehumbert, 1997). Thus, this sufficient temperature homogenization in the lower troposphere sustains states neutral to the growth of synoptic eddies but favorable to intraseasonal variability and the associated periodic behavior.

4 Conclusion and Discussion

We study the regional features of storm tracks' 20-30 day periodic variability in austral summer by applying the filtered variance approach to local wave activity. While the synoptic variance is largely zonally elongated over the storm track, we find a strong local enhancement of intraseasonal variability within the South Pacific with a minimum strength of the storm track. For this region, we find that this enhanced region is marked with local 20-30 day periodic behavior of precipitation and local wave activity whereby rejecting the 'null hypothesis' that intraseasonal variability is nothing more than a red-noise response to stochastic forcing by synoptic transients. The local periodicity is driven by enhanced variability of low-level eddy heat flux on the same timescale. The filtered variance of LWA analysis offers insights into the regional features of the coherent and slowly meandering structures of the circulation.

Internal modes of variability, such as BAM, result from the deterministic dynamics of the atmosphere. Thus a translation into regional scales may indicate unique predictability beyond the typical weather range. While the fundamental dynamics of BAM remain an open question, it is clear that cross-scale interactions between the synoptic and intraseasonal scales set the regional structure of this internal mode. The local nature of the 20-30 day periodicity identified by local wave activity provides a potential source of intraseasonal predictability for weather analysts and forecasters. As an internal mode that has yet to be tapped for extending the forecast beyond the typical weather range, more work is needed to connect this intraseasonal mode of variability with serial clustering of extreme weather events to quantify this potential regional predictability. In a warming climate, BAM is projected to increase its strength (Wang et al., 2018). A further implication of this work is the question of how the intraseasonal mode of variability and the associated regional impacts will evolve as climate changes. With the rapid development of high-resolution Earth system modeling, we are at a crucial era to deepen our understanding of the synoptic-intraseasonal interactions and the associated Earth system's regional variability and predictability.

5 Data Availability Statement

The authors acknowledge the use of NASA AMSR-E product for precipitation dataset: `https://www.earthdata.nasa.gov/sensors/amsr-e`, and ERA-Interim reanalysis dataset: `https://apps.ecmwf.int/datasets/data/interim-full-daily/`. The open repository including codes and related data for plotting key figures in this work is pasted here: `https://doi.org/10.5281/zenodo.7855573`

Acknowledgments

The authors acknowledge to NASA for providing AMSR-E precipitation observation and ECMWF for providing ERA-Interim reanalysis dataset.

References

Berbery, E. H., & Vera, C. S. (1996, February). Characteristics of the Southern Hemisphere Winter Storm Track with Filtered and Unfiltered Data. *Journal of the Atmospheric Sciences*, *53*(3), 468–481. Retrieved 2023-04-

16, from https://journals.ametsoc.org/view/journals/atsc/53/3/1520-0469_1996_053_0468_cotshw_2_0_co_2.xml (Publisher: American Meteorological Society Section: Journal of the Atmospheric Sciences) doi: 10.1175/1520-0469(1996)053⟨0468:COTSHW⟩2.0.CO;2

Blackmon, M. L., Lee, Y.-H., & Wallace, J. M. (1984, March). Horizontal Structure of 500 mb Height Fluctuations with Long, Intermediate and Short Time Scales. *Journal of the Atmospheric Sciences*, *41*(6), 961–980. Retrieved 2023-04-16, from https://journals.ametsoc.org/view/journals/atsc/41/6/1520-0469_1984_041_0961_hsomhf_2_0_co_2.xml (Publisher: American Meteorological Society Section: Journal of the Atmospheric Sciences) doi: 10.1175/1520-0469(1984)041⟨0961:HSOMHF⟩2.0.CO;2

Blackmon, M. L., Wallace, J. M., Lau, N.-C., & Mullen, S. L. (1977, July). An Observational Study of the Northern Hemisphere Wintertime Circulation. *Journal of the Atmospheric Sciences*, *34*(7), 1040–1053. Retrieved 2023-03-31, from https://journals.ametsoc.org/view/journals/atsc/34/7/1520-0469_1977_034_1040_aosotn_2_0_co_2.xml (Publisher: American Meteorological Society Section: Journal of the Atmospheric Sciences) doi: 10.1175/1520-0469(1977)034⟨1040:AOSOTN⟩2.0.CO;2

Chen, G., Lu, J., Burrows, D. A., & Leung, L. R. (2015). Local finite-amplitude wave activity as an objective diagnostic of midlatitude extreme weather. *Geophysical Research Letters*, *42*(24), 10,952–10,960. Retrieved 2023-03-24, from https://onlinelibrary.wiley.com/doi/abs/10.1002/2015GL066959 (_eprint: https://onlinelibrary.wiley.com/doi/pdf/10.1002/2015GL066959) doi: 10.1002/2015GL066959

Feldstein, S. B. (2000, December). The Timescale, Power Spectra, and Climate Noise Properties of Teleconnection Patterns. *Journal of Climate*, *13*(24), 4430–4440. Retrieved 2023-03-31, from https://journals.ametsoc.org/view/journals/clim/13/24/1520-0442_2000_013_4430_ttpsac_2.0.co_2.xml (Publisher: American Meteorological Society Section: Journal of Climate) doi: 10.1175/1520-0442(2000)013⟨4430:TTPSAC⟩2.0.CO;2

Green, J. S. A. (1977). The Weather During July 1976: Some Dynamical Considerations of the Drought. *Weather*, *32*(4), 120–126. Retrieved 2023-04-19, from https://onlinelibrary.wiley.com/doi/abs/10.1002/j.1477-8696.1977.tb04532.x (_eprint: https://onlinelibrary.wiley.com/doi/pdf/10.1002/j.1477-8696.1977.tb04532.x) doi: 10.1002/j.1477-8696.1977.tb04532.x

Hartmann, D. L. (2015). *Global Physical Climatology: Second Edition* (2nd ed ed.). Kent: Elsevier Science & Technology. Retrieved 2023-04-16, from https://public.ebookcentral.proquest.com/choice/publicfullrecord.aspx?p=5754480 (OCLC: 1099348114)

Hasselmann, K. (1976). Stochastic climate models Part I. Theory. *Tellus*, *28*(6), 473–485. Retrieved 2023-04-19, from https://onlinelibrary.wiley.com/doi/abs/10.1111/j.2153-3490.1976.tb00696.x (_eprint: https://onlinelibrary.wiley.com/doi/pdf/10.1111/j.2153-3490.1976.tb00696.x) doi: 10.1111/j.2153-3490.1976.tb00696.x

Held, I. M. (1999, January). The macroturbulence of the troposphere. *Tellus A: Dynamic Meteorology and Oceanography*, *51*(1), 59–70. Retrieved 2023-04-19, from https://doi.org/10.3402/tellusa.v51i1.12306 (Publisher: Taylor & Francis _eprint: https://doi.org/10.3402/tellusa.v51i1.12306) doi: 10.3402/tellusa.v51i1.12306

Huang, C. S. Y., & Nakamura, N. (2016, January). Local Finite-Amplitude Wave Activity as a Diagnostic of Anomalous Weather Events. *Journal of the Atmospheric Sciences*, *73*(1), 211–229. Retrieved 2023-03-24, from https://journals.ametsoc.org/view/journals/atsc/73/1/jas-d-15-0194.1.xml (Publisher: American Meteorological Society Section: Journal of the Atmospheric Sciences) doi: 10.1175/JAS-D-15-0194.1

Huang, C. S. Y., & Nakamura, N. (2017). Local wave activity budgets of the wintertime Northern Hemisphere: Implication for the Pacific and Atlantic storm tracks. *Geophysical Research Letters*, *44*(11), 5673–5682. Retrieved 2023-03-31, from https://onlinelibrary.wiley.com/doi/abs/10.1002/2017GL073760 (_eprint: https://onlinelibrary.wiley.com/doi/pdf/10.1002/2017GL073760) doi: 10.1002/2017GL073760

Kidson, J. W. (1991, September). Intraseasonal Variations in the Southern Hemisphere Circulation. *Journal of Climate*, *4*(9), 939–953. Retrieved 2023-04-16, from https://journals.ametsoc.org/view/journals/clim/4/9/1520-0442_1991_004_0939_ivitsh_2_0_co_2.xml (Publisher: American Meteorological Society Section: Journal of Climate) doi: 10.1175/1520-0442(1991)004⟨0939:IVITSH⟩2.0.CO;2

Kushner, P. J., & Held, I. M. (1998). A test, using atmospheric data, of a method for estimating oceanic eddy diffusivity. *Geophysical Research Letters*, *25*(22), 4213–4216. Retrieved 2023-04-19, from https://onlinelibrary.wiley.com/doi/abs/10.1029/1998GL900142 (_eprint: https://onlinelibrary.wiley.com/doi/pdf/10.1029/1998GL900142) doi: 10.1029/1998GL900142

Leith, C. E. (1973, September). The Standard Error of Time-Average Estimates of Climatic Means. *Journal of Applied Meteorology and Climatology*, *12*(6), 1066–1069. Retrieved 2023-04-19, from https://journals.ametsoc.org/view/journals/apme/12/6/1520-0450_1973_012_1066_tseota_2_0_co_2.xml (Publisher: American Meteorological Society Section: Journal of Applied Meteorology and Climatology) doi: 10.1175/1520-0450(1973)012⟨1066:TSEOTA⟩2.0.CO;2

Lorenz, D. J., & Hartmann, D. L. (2001, November). Eddy–Zonal Flow Feedback in the Southern Hemisphere. *Journal of the Atmospheric Sciences*, *58*(21), 3312–3327. Retrieved 2023-03-31, from https://journals.ametsoc.org/view/journals/atsc/58/21/1520-0469_2001_058_3312_ezffit_2.0.co_2.xml (Publisher: American Meteorological Society Section: Journal of the Atmospheric Sciences) doi: 10.1175/1520-0469(2001)058⟨3312:EZFFIT⟩2.0.CO;2

Nakamura, H., & Shimpo, A. (2004, May). Seasonal Variations in the Southern Hemisphere Storm Tracks and Jet Streams as Revealed in a Reanalysis Dataset. *Journal of Climate*, *17*(9), 1828–1844. Retrieved 2023-04-16, from https://journals.ametsoc.org/view/journals/clim/17/9/1520-0442_2004_017_1828_svitsh_2.0.co_2.xml (Publisher: American Meteorological Society Section: Journal of Climate) doi: 10.1175/1520-0442(2004)017⟨1828:SVITSH⟩2.0.CO;2

Nakamura, N., & Zhu, D. (2010, September). Finite-Amplitude Wave Activity and Diffusive Flux of Potential Vorticity in Eddy–Mean Flow Interaction. *Journal of the Atmospheric Sciences*, *67*(9), 2701–2716. Retrieved 2023-03-24, from https://journals.ametsoc.org/view/journals/atsc/67/9/2010jas3432.1.xml (Publisher: American Meteorological Society Section: Journal of the Atmospheric Sciences) doi: 10.1175/2010JAS3432.1

Swanson, K. L., & Pierrehumbert, R. T. (1997, June). Lower-Tropospheric Heat Transport in the Pacific Storm Track. *Journal of the Atmospheric Sciences*, *54*(11), 1533–1543. Retrieved 2023-04-19, from https://journals.ametsoc.org/view/journals/atsc/54/11/1520-0469_1997_054_1533_lthtit_2.0.co_2.xml (Publisher: American Meteorological Society Section: Journal of the Atmospheric Sciences) doi: 10.1175/1520-0469(1997)054⟨1533:LTHTIT⟩2.0.CO;2

Thompson, D. W. J., & Barnes, E. A. (2014, February). Periodic Variability in the Large-Scale Southern Hemisphere Atmospheric Circulation. *Science*, *343*(6171), 641–645. Retrieved 2023-03-24, from https://www.science.org/doi/10.1126/science.1247660 (Publisher: American Association for the

Advancement of Science) doi: 10.1126/science.1247660

Thompson, D. W. J., Crow, B. R., & Barnes, E. A. (2017, March). Intraseasonal Periodicity in the Southern Hemisphere Circulation on Regional Spatial Scales. *Journal of the Atmospheric Sciences*, *74*(3), 865–877. Retrieved 2023-03-31, from `https://journals.ametsoc.org/view/journals/atsc/74/3/jas-d-16-0094.1.xml` (Publisher: American Meteorological Society Section: Journal of the Atmospheric Sciences) doi: 10.1175/JAS-D-16-0094.1

Thompson, D. W. J., & Woodworth, J. D. (2014, April). Barotropic and Baroclinic Annular Variability in the Southern Hemisphere. *Journal of the Atmospheric Sciences*, *71*(4), 1480–1493. Retrieved 2023-03-31, from `https://journals.ametsoc.org/view/journals/atsc/71/4/jas-d-13-0185.1.xml` (Publisher: American Meteorological Society Section: Journal of the Atmospheric Sciences) doi: 10.1175/JAS-D-13-0185.1

Trenberth, K. E. (1981). Seasonal variations in global sea level pressure and the total mass of the atmosphere. *Journal of Geophysical Research: Oceans*, *86*(C6), 5238–5246. Retrieved 2023-04-16, from `https://onlinelibrary.wiley.com/doi/abs/10.1029/JC086iC06p05238` (_eprint: https://onlinelibrary.wiley.com/doi/pdf/10.1029/JC086iC06p05238) doi: 10.1029/JC086iC06p05238

Trenberth, K. E. (1991, October). Storm Tracks in the Southern Hemisphere. *Journal of the Atmospheric Sciences*, *48*(19), 2159–2178. Retrieved 2023-04-16, from `https://journals.ametsoc.org/view/journals/atsc/48/19/1520-0469_1991_048_2159_stitsh_2_0_co_2.xml` (Publisher: American Meteorological Society Section: Journal of the Atmospheric Sciences) doi: 10.1175/1520-0469(1991)048⟨2159:STITSH⟩2.0.CO;2

Vitart, F., Ardilouze, C., Bonet, A., Brookshaw, A., Chen, M., Codorean, C., … Zhang, L. (2017, January). The Subseasonal to Seasonal (S2S) Prediction Project Database. *Bulletin of the American Meteorological Society*, *98*(1), 163–173. Retrieved 2023-03-31, from `https://journals.ametsoc.org/view/journals/bams/98/1/bams-d-16-0017.1.xml` (Publisher: American Meteorological Society Section: Bulletin of the American Meteorological Society) doi: 10.1175/BAMS-D-16-0017.1

Wang, L., Lu, J., & Kuang, Z. (2018). A Robust Increase of the Intraseasonal Periodic Behavior of the Precipitation and Eddy Kinetic Energy in a Warming Climate. *Geophysical Research Letters*, *45*(15), 7790–7799. Retrieved 2023-03-24, from `https://onlinelibrary.wiley.com/doi/abs/10.1029/2018GL078495` (_eprint: https://onlinelibrary.wiley.com/doi/pdf/10.1029/2018GL078495) doi: 10.1029/2018GL078495

Wang, L., & Nakamura, N. (2015). Covariation of finite-amplitude wave activity and the zonal mean flow in the midlatitude troposphere: 1. Theory and application to the Southern Hemisphere summer. *Geophysical Research Letters*, *42*(19), 8192–8200. Retrieved 2023-04-16, from `https://onlinelibrary.wiley.com/doi/abs/10.1002/2015GL065830` (_eprint: https://onlinelibrary.wiley.com/doi/pdf/10.1002/2015GL065830) doi: 10.1002/2015GL065830

Wang, L., & Nakamura, N. (2016, December). Covariation of Finite-Amplitude Wave Activity and the Zonal-Mean Flow in the Midlatitude Troposphere. Part II: Eddy Forcing Spectra and the Periodic Behavior in the Southern Hemisphere Summer. *Journal of the Atmospheric Sciences*, *73*(12), 4731–4752. Retrieved 2023-04-22, from `https://journals.ametsoc.org/view/journals/atsc/73/12/jas-d-16-0091.1.xml` (Publisher: American Meteorological Society Section: Journal of the Atmospheric Sciences) doi: 10.1175/JAS-D-16-0091.1

Xue, D., Lu, J., Qian, Y., & Zhang, Y. (2021). Evidence for Coupling Between the Subseasonal Oscillations in the Southern Hemisphere Midlatitude Ocean and Atmosphere. *Journal of Geophysical Research: Atmospheres*, *126*(4), e2020JD033872. Retrieved 2023-03-31, from `https://onlinelibrary.wiley.com/doi/abs/10.1029/2020JD033872` (_eprint: https://onlinelibrary.wiley.com/doi/pdf/10.1029/2020JD033872) doi: 10.1029/2020JD033872

Regional Features of the 20-30 Day Periodic Behavior in the Southern Hemisphere Summer Circulation

Zhaoyu Liu[1], Lei Wang[1]

[1]Department of Earth, Atmospheric, and Planetary Sciences, Purdue University

Key Points:

- The hemispheric 20-30 day periodicity in the austral summer has a strong localization in local wave activity and precipitation.
- Strong enhancement of intraseasonal variability and local periodic behavior is identified within the South Pacific.
- The local nature of 20-30 day periodicity offers a potential source of intraseasonal predictability for weather analysts and forecasters.

Corresponding author: Lei Wang, leiwang@purdue.edu

Abstract

The Southern Hemispheric (SH) storm tracks exhibit a robust intraseasonal periodicity of 20-30 days as the leading mode of zonal-mean eddy kinetic energy. To what extent this hemispheric-scale mode of variability translates to smaller scales remains debated. This work studies the regional features of SH storm tracks through the filtered variance of local finite-amplitude wave activity. While the synoptic variance is zonally elongated over the storm track, we find a strong enhancement of intraseasonal variability within the South Pacific with a minimum strength of the storm track. This enhanced region is marked with 20-30 day periodic behavior of local wave activity and precipitation and is driven by enhanced variability of low-level eddy heat flux on the same timescale. The local nature of 20-30 day periodicity offers a potential source of intraseasonal predictability for weather analysts and forecasters.

Plain Language Summary

Storm activities in Southern Hemisphere (SH) midlatitudes are characterized by 20-30 day periodic behavior, representing a hemispheric-scale pulsing of zonal-mean extratropical eddy activity. This phenomenon has been termed the Baroclinic Annular Mode (BAM) defined as the leading EOF mode of the zonal-mean eddy kinetic energy. If this large-scale mode were to have a strong local nature, such periodic behavior in subseasonal-to-seasonal time scale would have important implications for understanding and predicting the medium-range weather system, especially for extreme events. However, to what extent we can identify regional features of such hemispheric-scale mode of variability remains unclear.

We demonstrate the regional feature of this periodic variability by showing the variance of local wave activity in different time scales. We find that the variability in a shorter weather time scale (2-7 days) exhibits a largely zonally-symmetric structure, but the variability in the intraseasonal time scale exhibits a strong localization concentrated in the South Pacific. We further assess the distribution of periodicity within the intraseasonal variability and find that the 20-30 day periodicity is also localized within South Pacific. The local nature of this 20-30 day periodicity indicates the potential utility of the BAM for weather analysts and forecasters.

1 Introduction

High-quality societal applications for decision-makers for optimizing resource management and preventing disaster require accurate sub-seasonal to seasonal (S2S, intraseasonal) predictions, because high-impact extreme weather events, such as long-lasting heatwaves and extreme cold spells, often occur on this timescale. Recent research has identified multiple sources of S2S predictability, such as the Madden-Julian oscillation (MJO), the basic state of the ENSO, soil moisture, tropical-extratropical teleconnections, etc (see the review in (Vitart et al., 2017)). However, nearly all of these sources are outside of the midlatitude internal dynamics. This is due to the conventional understanding that the large-scale midlatitude variability is typically consistent with Gaussian red noise rather than periodic behaviors (Feldstein, 2000; Lorenz & Hartmann, 2001). As a 'null hypothesis,' intraseasonal variability can be considered as a response to stochastic forcing by higher-frequency synoptic system's disturbances (Leith, 1973; Hasselmann, 1976; Green, 1977). Assuming synoptic disturbances as Gaussian white noise forcing F_t, this 'null hypothesis' suggests the time series of intraseasonal variability x_t as a Gaussian red noise process $x_t = \alpha x_{t-1} + F_t$, where α is a positive constant defining the e-folding timescale of the intraseasonal variability. Hence, no unique source of predictability on regional scales has been identified within the midlatitude atmosphere beyond the synoptic weather range.

Baroclinic Annular Mode (BAM), however, a recently discovered large-scale mid-latitude variability over the SH, is characterized by a robust intraseasonal periodicity about 20-30 day (Thompson & Barnes, 2014; Thompson & Woodworth, 2014). BAM is defined by the leading empirical orthogonal function (EOF) of the zonal-mean eddy kinetic energy (EKE), representing the intraseasonal oscillation of eddy activity on a hemispheric scale. If such periodic nature were to translate to smaller scales at certain regions, it could serve as a new source of S2S predictability. In a regional scale study of BAM, Thompson et al. (2017) find that the periodicity in the upper troposphere eddy kinetic energy is not apparent at a fixed location. As the averaging windows reduce from the entire global circle to 30-degree wide regions, the power spectra reduce from a robust quasi-periodic shape to a red noise without any major enhancement of the variance on the 20-30 day frequency range. The discovery of the lack of local periodicity for regions smaller than 30 degrees is explained through a conceptual model featuring out-of-phase anomalies between the upper and lower troposphere. A similar finding was also confirmed in Xue et al. (2021), that the domain should be wide enough to accommodate a wave packet so that the intraseasonal periodicity can be identified. Therefore, as the averaging domain size reduces to smaller scales, periodic behavior at a fixed region is not expected, which is consistent with the above 'null hypothesis.' To what extent such a leading mode of variability is translated to regional scale intraseasonal variability - and thus modulating serial clustering of extreme weather events - remains an open question.

To address this question, we will adopt a filtered variance approach, which has been well-developed to identify the geographic distributions of the storm tracks (Blackmon et al., 1977). Typically, a scalar quantity combining multiple information is preferred, such as the 500 hPa geopotential height field (Z500), which is related to both the wind and temperature. Blackmon et al. (1977) developed this filtered variance framework using the Northern Hemisphere (NH) Z500, with the spectral domains separated into synoptic and intraseasonal bands, respectively (also see Blackmon et al. (1984)). Through a similar filtered variance analysis, Trenberth (1981, 1991) studied the SH circulation within synoptic time scales and found that the SH storm tracks exhibit strong zonal symmetry along with a maximum located at the Southern Indian Ocean and a minimum at the South Pacific. Kidson (1991) found a zonal-symmetric pattern for the intraseasonal variability in the SH (see also Hartmann (2015)). Therefore, we aim to make progress on deepening the understanding of the regional features of the intraseasonal variability - a less explored territory. Specifically, we ask: are these regions with enhanced intraseasonal variance mainly characterized by a Gaussian red-noise spectrum as expected from the 'null hypothesis,' or have certain quasi-periodic behaviors that may be connected with the hemispheric-scale 20-30 day periodic mode of variability?

To answer this question, we start with the surface precipitation analysis, a directly measured quantity as a surrogate for the local behavior of storm activities. Then we will quantify the regional variability pattern by applying the filtered variance approach (Blackmon et al., 1977) to key representative variables, including Z500, EKE, and a newly developed quantity local wave activity (LWA), as well as the low-level eddy heat flux that drives LWA tendency. This work focuses on Austral summer season (DJF) since the periodic behavior is much more significant in austral summer than other seasons (Wang & Nakamura, 2015). Comparisons to the Northern Hemisphere and with different seasons will be addressed in follow-up studies. The paper is organized as follows. In Section 2, we introduce data and key methodologies such as LWA and filtered variance framework. In Section 3, we first discuss the regional features of surface precipitation and then demonstrate the synoptic and intraseasonal variability patterns of different variables associated with spectral analysis. Section 4 concludes with a summary.

2 Data and Method

We use ECMWF-Interim reanalysis products, including zonal and meridional velocities, air temperature, and geopotential height, with a horizontal resolution $1.25^\circ \times 1.25^\circ$ and daily resolution from 1979 to 2018. Additionally, the daily precipitation is obtained from the Advanced Microwave Scanning Radiometer(AMSR) -E from 2003 to 2010 processed by a three-day moving average. AMSR-E measures the surface rain rate covering from 70°N-70°S.

The filtered variability approach is based on the standard deviation in the 2-7 day band for synoptic analysis and the 10-45 day band for intraseasonal analysis. The temporal filter is based on Fast Fourier Transform (FFT) with Hanning window from 1 December to 28 February between 1979 and 2018. The framework is applied to Z500, EKE, LWA, and 850hPa eddy heat flux, respectively. EKE is defined as $((u^*)^2+(v^*)^2)/2$ and is averaged with density weighting along the vertical column. 850hPa eddy heat flux is defined as v^*T^*, where the asterisks represent the departures from the zonal mean.

Unlike EKE, local finite-amplitude wave activity emphasizes on coherent meandering of the contours of a quasi-conserved quantity. Conserving flow circulation through Kelvin's circulation theorem, the area bounded by the reference quantity contour is the same as the one bounded by the latitude circle. Finite-amplitude wave activity (FAWA, see N. Nakamura and Zhu (2010)) focuses on the total displacement over the entire longitudes, while LWA (see Huang and Nakamura (2016), Chen et al. (2015)) measures the displacement for each longitude, so that a full longitude-latitude pattern of wave activity can be quantified. For example, the field of Z500 can be used to define the local wave activity (Chen et al., 2015):

$$A_{z500}(\phi_e, \lambda, t) = \frac{a}{cos\phi_e}\left(\int_{z' \geq 0, \phi \leq \phi_e, \lambda = const} z' cos\phi d\phi - \int_{z' \leq 0, \phi \geq \phi_e, \lambda = const} z' cos\phi d\phi\right), \quad (1)$$

where a is the earth radius, ϕ, λ, represents the latitude and longitude respectively, $z' = z - Z(\phi_e)$ is the deviation from the reference Z500 contour $Z(\phi_e)$ at its equivalent latitude ϕ_e. The relation between $Z(\phi_e)$ and ϕ_e is connected by the same bounded area $\phi_e(Z) = arcsin[1 - \frac{S(Z)}{2\pi a^2}]$.

A quasi-geostrophic potential vorticity (QGPV) -based LWA allows one to quantify the role of eddy forcing. Local wave activity at each pseudo-height level can be assessed independently, and the density-weighted vertically averaged value is used to represent the barotropic wave activity. See supplementary material for more details.

3 Results

We start with analyzing the temporal and spatial features of precipitation, since surface rain rate is a directly measured quantity by space-based meteorological satellites, and is highly correlated with the variability of storm activity. Thompson and Barnes (2014) found that the mid-latitude mean precipitation can also exhibit a significant intraseasonal periodicity around 20-30 days as a key feature of BAM. Is there any localization of such periodic behavior in the precipitation?

To illustrate the regional feature, we calculated the power spectra of surface rain rate retrieved from AMSR-E in four separated regions as shown in Figure 1c: 0°-90°E, 90°E-180°, 180°-90°W, 90°W-0°, all of which are averaged between 40°S-50°S, and we find that the most significant 20-30 day periodicity is located at the South Pacific (180°-90°W with 95% confidence level), while spectra features in other three regions are mainly characterized by enhanced synoptic variability (0°-180°E) or similar to a red-noise (90°W-0°). Thus, there is a localization of the surface rain rate's 20-30 day periodic behavior. Is this localization of rain rate periodicity a coincidence? Or it implies a strong local-

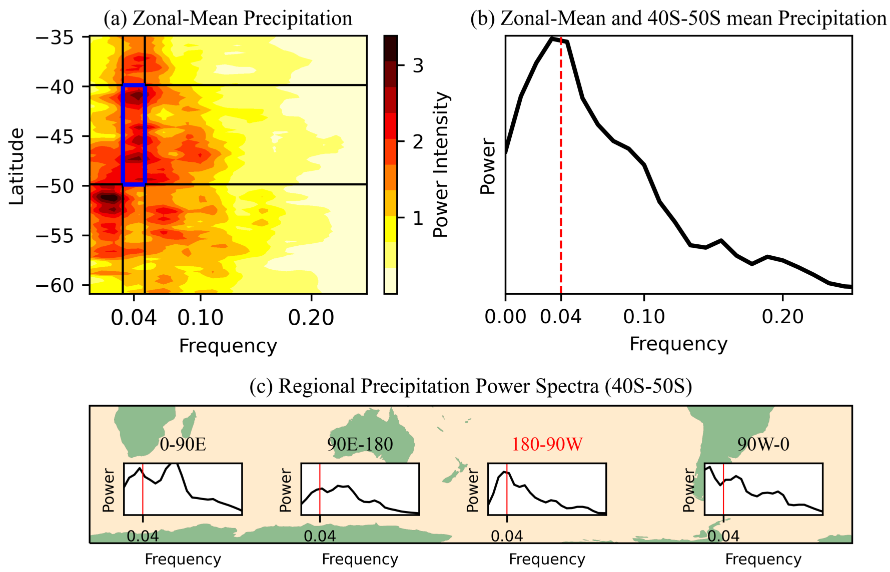

Figure 1: Power spectra of surface precipitation in austral summer(DJF) from 2002-2010 for (a)zonal-mean, (b)zonal-mean and averaged between 40°S-50°S, (c)regional mean of 0°-90°E, 90°E-180°, 180°-90°W, 90°W-0°, all of which averaged between 40°S-50°S.

ization of the 20-30 day periodic behavior for the underlying large-scale atmospheric circulation?

We adopt the filtered variance approach of Blackmon et al. (1977) to quantify the regional features of synoptic and intraseasonal variability, respectively. The variability of Z500 exhibits a more zonally symmetric regional pattern within both synoptic and intraseasonal timescales as consistent with the previous work (see Supplementary Figure S1). Centered around 50°S, the synoptic variance is strongest in the South Indian Ocean, while the maximum of intraseasonal variance is zonally elongated over much of the South Pacific. The zonal-mean Z500 field does not show any periodic behavior in the intraseasonal timescales (see Supplementary Figure S2), thus we would not expect any local periodic behavior in the Z500 field.

As the variable central to the BAM definition, zonal-mean EKE is characterized by a robust periodic behavior (Thompson & Woodworth, 2014). However, as Thompson et al. (2017) discovered, the periodicity in EKE is not apparent at a fixed location, and we find consistent results that the regional variability is much weaker in the intraseasonal band at pixel(i.e., grid point) level (see Supplementary Figure S3). Instead, a two-branch structure is observed in the intraseasonal variance pattern of EKE, and can be attributed to the intense wave-breaking processes at the South Pacific that generate intense local values of zonal and meridional velocities, since qualitatively speaking, EKE reaches maximum where the circulation contours are the densest. The two-branch structure belongs to the same storm activity region - as the below LWA analysis would illustrate more clearly.

Therefore, an accurate diagnostic approach for eddy activity that can illustrate both spatial and temporal features is required to study our key question. As a comparison with Z500 or EKE, the local finite-amplitude wave activity (LWA) provides a more objective

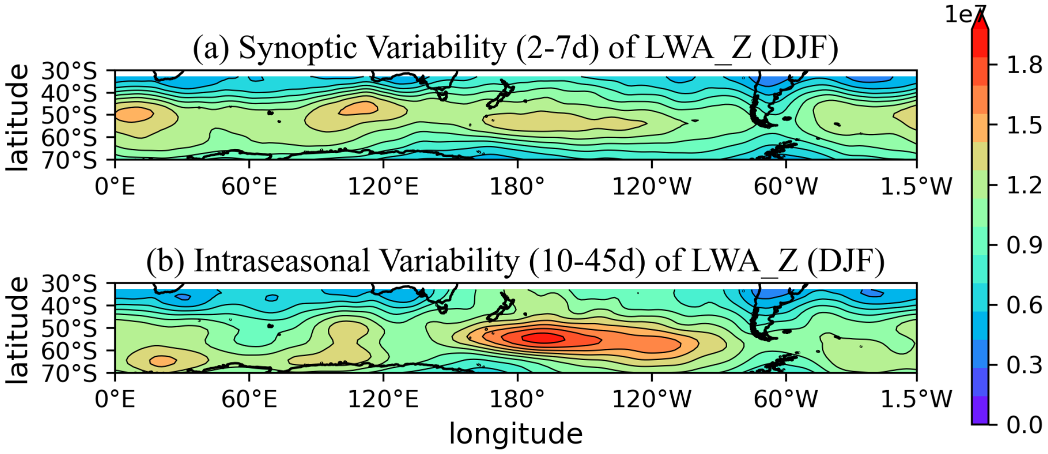

Figure 2: Bandpass-filtered variance converted to standard deviation for Z500_based LWA (LWA_Z) in austral summer(DJF): (a)synoptic variability(2-7 days), and (b)intraseasonal variability(10-45 days). The shading represents values between $0m^2$ and $1.9 \times 10^7 m^2$.

approach for the diagnostic of eddy activity. QGPV-based LWA is a conserved quantity and driven by eddy flux terms - each bearing clear physical interpretations, directly representing the pseudo-momentum carried by eddy. Z500-based LWA shares many features of the QGPV-based LWA, and it is more straightforward to calculate. Regarding the spatial feature, LWA can capture the breaking waves as part of an underlying coherent pattern (see the comparison between LWA and EKE in Huang and Nakamura (2017)). For example, for a large-scale dipole structure, the maximum value of LWA locates only at the center of the overturning contours of PV (or Z500). In contrast, the maximum values of EKE are found at two distinct places - the edge of the upper high-pressure system and the edge of the lower low-pressure system. Regarding the temporal feature, Wang and Nakamura (2015) confirmed that FAWA also exhibits a robust 20-30 day periodicity, consistent with features of BAM defined by the EOF-based EKE framework. Since zonal-average of LWA naturally conforms to FAWA, LWA has the strength to pinpoint regional features more precisely, and to allow for a direct connection with the hemispheric-scale 20-30 day periodic behavior as defined by FAWA. Both the QGPV and Z500 fields can be used to calculate the LWA, with the former directly connected with the eddy fluxes terms and the latter more commonly available among climate model outputs. Our analysis confirms that both approaches yield qualitatively consistent results.

Figure 2 shows the synoptic and intraseasonal variability pattern of Z500-based LWA in austral summer. The synoptic variability still exhibits a zonally symmetric pattern, with the maximum variance concentrated in the Southeast (SE) Indian Ocean as well as in the SE Atlantic, and the minimum variance in the SE Pacific close to South America (also see Supplementary Figure S4 for QGPV-based LWA). This result is qualitatively consistent with the pattern shown by the filtered variance of the Z500 field, but further captures a more detailed and coherent structure clearly emphasizing the maximum region. Such intensified synoptic variability at the SE Indian Ocean and Atlantic can be largely attributed to the downstream development of baroclinic waves (Berbery & Vera, 1996), and therefore the largest synoptic variance is expected to occur closely downstream to the regions of maximum observed baroclinicity, which is located at the Southwest (SW) Indian Ocean and SW Atlantic (the sea surface temperature frontal zones, see H. Naka-

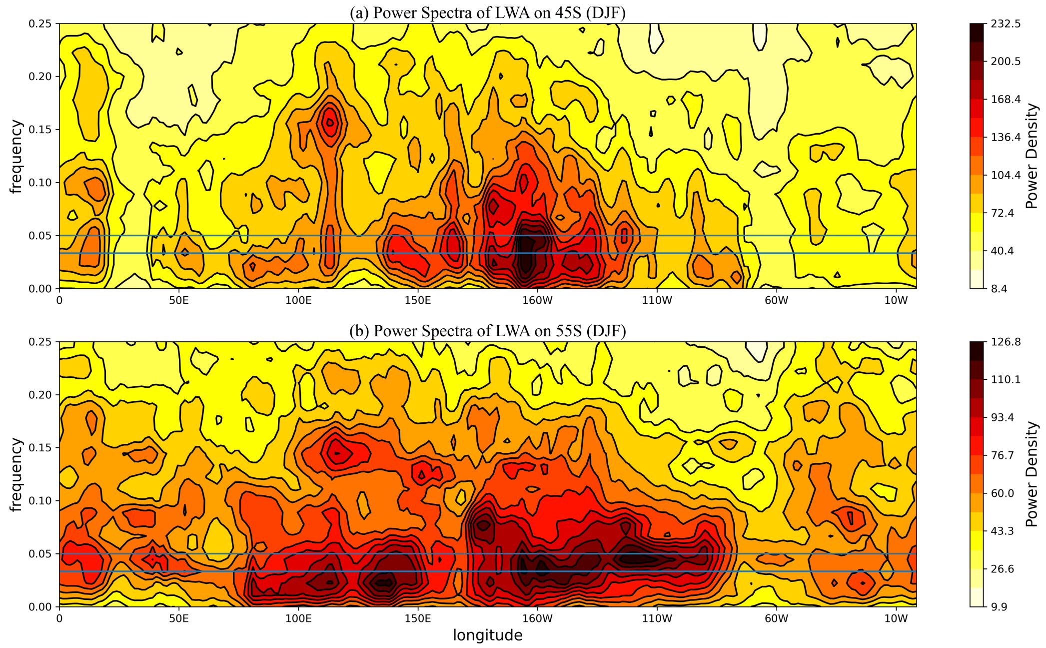

Figure 3: Power spectra of QGPV-based LWA as functions of longitude and frequency at two representative latitudes 45°S (upper panel) and 55°S (lower panel), respectively.

mura and Shimpo (2004)). The weakened synoptic signal at the South Pacific is associated with the decaying process of extratropical cyclones' lifecycles.

With an ability to capture larger-scale meandering, the filtered variance of Z500-based LWA captures the corresponding intraseasonal variability more efficiently than that of the Z500 and EKE field. As shown in Figure 2b, the intraseasonal variance of LWA is near twice its synoptic counterpart. Besides, the intraseasonal pattern is not as zonally-elongated as the synoptic variance or the pattern captured by Z500. In contrast, a strong local enhancement is found confined at the South Pacific, largely within 180°-150°W and 50°S-60°S. This region is right at the center between the two branches shown in the intraseasonal pattern of EKE (Supplementary Figure S3b), which demonstrates the advantage of LWA in capturing coherent patterns for large-scale eddies. Similarly, the filtered variance of QGPV-based LWA shows consistent results: a robust intensification of intraseasonal variability at the South Pacific is observed located within 180°-150°W (see Supplementary Figure S4b). Despite the minor difference that the QGPV-based LWA shows a more equatorward intraseasonal pattern, both types of the filtered variance of LWA show a consistent key region of intraseasonal variability of storm activities confined within the South Pacific.

With a region of enhanced intraseasonal variance pinned down, we next investigate whether the enhanced frequencies is related to the 20-30 day periodic mode. To zoom into the crucial latitudes where such periodicity is concentrated. Figure 3 shows the power spectra of QGPV-based LWA as the function of longitudes and frequencies at 45°S and 55°S, since Wang and Nakamura (2015) found that the 20-30 day periodic variability mainly dominates the midlatitudes from 40°S-60°S (also see Supplementary Figure S5). Within the intraseasonal domain, the 20-30 day periodicity (0.03-0.05 cpd, bounded by two blue

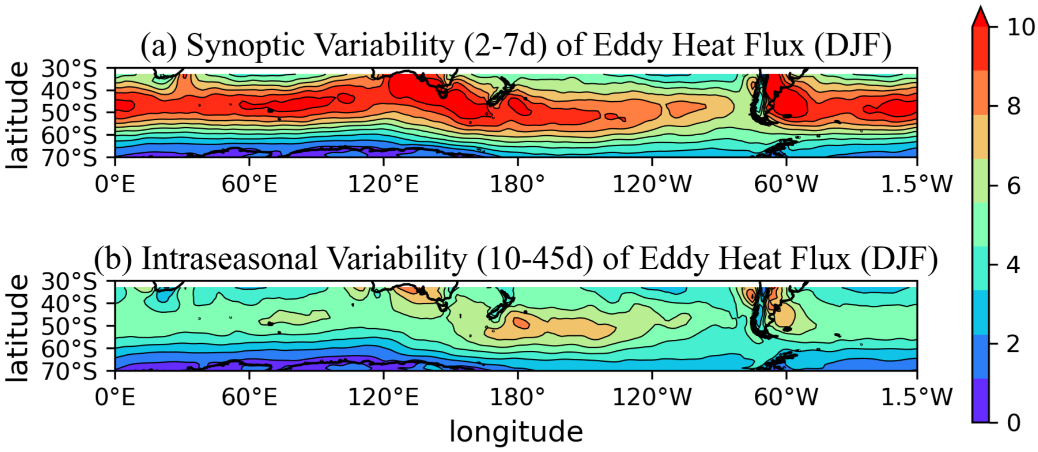

Figure 4: Bandpass-filtered variance converted to standard deviation for 850hPa eddy heat flux in austral summer(DJF): (a)synoptic variability(2-7 days), and (b)intraseasonal variability(10-45 days). The shading represents values between $0mK/s$ and $10mK/s$.

lines in Figure 3) exhibits a strong localization as hinted by the filtered variance approach. At 45°S for example, the strongest 20-30 day frequency band is largely confined between 180°-150°W, overlapping the region where the intrasesonal variance reaches its maximum (shown in Figure 2b). This regional feature of periodicity might slightly vary with different latitudes, for example the most significant 20-30 day periodicity at 55°S exhibits an elongated range covering 180°-100°W. By and large, all cross sections within midlatitudes demonstrate that the 20-30 day periodicity has a strong regional preference located at the South Pacific. A similar result can be observed if the LWA is meridionally averaged between 40°S-60°S (see Supplementary Figure S6), the 20-30 day periodicity is still strongly localized at the South Pacific, resembling the pattern at individual latitudes. Note that, in this case, the budget term of meridional eddy momentum flux is removed due to the meridional average, and therefore it can suggests that, the meridional eddy momentum flux plays a non-dominant role in the intraseasonal variability. The zonal wave flux convergence, as another important budget term of LWA, will not directly impact LWA's intraseasonal variability neither, as the zonal wave flux convergence primarily populate the synoptic variability of wave activity (Huang & Nakamura, 2017). The cross-section of power spectra for Z500-based LWA shows similar results to the QGPV-based LWA, whereas that for EKE does not show robust 20-30 day periodicity (see Supplementary Figure S7 and S8).

What would be a key factor that drives such locally confined intraseasonal variability including the 20-30 day periodicity? Wang and Nakamura (2015, 2016) find that eddy forcing due to the low-level eddy heat flux drives the 20-30 day periodicity in zonal-mean of LWA (i.e., FAWA). A local enhanced variance of eddy heat flux should be expected if this can also translate into regional scales. Figure 4 confirmed this expectation by showing that the intraseasonal variance of 850hPa eddy heat flux is also localized between 180°-150°W, largely overlapping the region where the intraseasonal variance of LWA is strongly enhanced, as shown in Figures 2 and 3. The cross-section power spectra of 850 hPa eddy heat flux further indicates that the low-level eddy heat flux also exhibits enhanced 20-30 day periodicity at fixed locations, largely confined within the South Pacific as well (see Supplementary Figure S9). This locally enhanced intraseasonal variability of 850hPa eddy heat flux is marked with a strong r.m.s. eddy streamfunction as a surrogate of eddy diffusivity for estimating the horizontal eddy heat flux (Kushner &

Held, 1998; Held, 1999). Strong thermal damping over this area reduces linear baroclinic eddy growth rates (Swanson & Pierrehumbert, 1997). Thus, this sufficient temperature homogenization in the lower troposphere sustains states neutral to the growth of synoptic eddies but favorable to intraseasonal variability and the associated periodic behavior.

4 Conclusion and Discussion

We study the regional features of storm tracks' 20-30 day periodic variability in austral summer by applying the filtered variance approach to local wave activity. While the synoptic variance is largely zonally elongated over the storm track, we find a strong local enhancement of intraseasonal variability within the South Pacific with a minimum strength of the storm track. For this region, we find that this enhanced region is marked with local 20-30 day periodic behavior of precipitation and local wave activity whereby rejecting the 'null hypothesis' that intraseasonal variability is nothing more than a red-noise response to stochastic forcing by synoptic transients. The local periodicity is driven by enhanced variability of low-level eddy heat flux on the same timescale. The filtered variance of LWA analysis offers insights into the regional features of the coherent and slowly meandering structures of the circulation.

Internal modes of variability, such as BAM, result from the deterministic dynamics of the atmosphere. Thus a translation into regional scales may indicate unique predictability beyond the typical weather range. While the fundamental dynamics of BAM remain an open question, it is clear that cross-scale interactions between the synoptic and intraseasonal scales set the regional structure of this internal mode. The local nature of the 20-30 day periodicity identified by local wave activity provides a potential source of intraseasonal predictability for weather analysts and forecasters. As an internal mode that has yet to be tapped for extending the forecast beyond the typical weather range, more work is needed to connect this intraseasonal mode of variability with serial clustering of extreme weather events to quantify this potential regional predictability. In a warming climate, BAM is projected to increase its strength (Wang et al., 2018). A further implication of this work is the question of how the intraseasonal mode of variability and the associated regional impacts will evolve as climate changes. With the rapid development of high-resolution Earth system modeling, we are at a crucial era to deepen our understanding of the synoptic-intraseasonal interactions and the associated Earth system's regional variability and predictability.

5 Data Availability Statement

The authors acknowledge the use of NASA AMSR-E product for precipitation dataset: `https://www.earthdata.nasa.gov/sensors/amsr-e`, and ERA-Interim reanalysis dataset: `https://apps.ecmwf.int/datasets/data/interim-full-daily/`. The open repository including codes and related data for plotting key figures in this work is pasted here: `https://doi.org/10.5281/zenodo.7855573`

Acknowledgments

The authors acknowledge to NASA for providing AMSR-E precipitation observation and ECMWF for providing ERA-Interim reanalysis dataset.

References

Berbery, E. H., & Vera, C. S. (1996, February). Characteristics of the Southern Hemisphere Winter Storm Track with Filtered and Unfiltered Data. *Journal of the Atmospheric Sciences*, *53*(3), 468–481. Retrieved 2023-04-

16, from https://journals.ametsoc.org/view/journals/atsc/53/3/1520-0469_1996_053_0468_cotshw_2_0_co_2.xml (Publisher: American Meteorological Society Section: Journal of the Atmospheric Sciences) doi: 10.1175/1520-0469(1996)053⟨0468:COTSHW⟩2.0.CO;2

Blackmon, M. L., Lee, Y.-H., & Wallace, J. M. (1984, March). Horizontal Structure of 500 mb Height Fluctuations with Long, Intermediate and Short Time Scales. *Journal of the Atmospheric Sciences*, *41*(6), 961–980. Retrieved 2023-04-16, from https://journals.ametsoc.org/view/journals/atsc/41/6/1520-0469_1984_041_0961_hsomhf_2_0_co_2.xml (Publisher: American Meteorological Society Section: Journal of the Atmospheric Sciences) doi: 10.1175/1520-0469(1984)041⟨0961:HSOMHF⟩2.0.CO;2

Blackmon, M. L., Wallace, J. M., Lau, N.-C., & Mullen, S. L. (1977, July). An Observational Study of the Northern Hemisphere Wintertime Circulation. *Journal of the Atmospheric Sciences*, *34*(7), 1040–1053. Retrieved 2023-03-31, from https://journals.ametsoc.org/view/journals/atsc/34/7/1520-0469_1977_034_1040_aosotn_2_0_co_2.xml (Publisher: American Meteorological Society Section: Journal of the Atmospheric Sciences) doi: 10.1175/1520-0469(1977)034⟨1040:AOSOTN⟩2.0.CO;2

Chen, G., Lu, J., Burrows, D. A., & Leung, L. R. (2015). Local finite-amplitude wave activity as an objective diagnostic of midlatitude extreme weather. *Geophysical Research Letters*, *42*(24), 10,952–10,960. Retrieved 2023-03-24, from https://onlinelibrary.wiley.com/doi/abs/10.1002/2015GL066959 (_eprint: https://onlinelibrary.wiley.com/doi/pdf/10.1002/2015GL066959) doi: 10.1002/2015GL066959

Feldstein, S. B. (2000, December). The Timescale, Power Spectra, and Climate Noise Properties of Teleconnection Patterns. *Journal of Climate*, *13*(24), 4430–4440. Retrieved 2023-03-31, from https://journals.ametsoc.org/view/journals/clim/13/24/1520-0442_2000_013_4430_ttpsac_2.0.co_2.xml (Publisher: American Meteorological Society Section: Journal of Climate) doi: 10.1175/1520-0442(2000)013⟨4430:TTPSAC⟩2.0.CO;2

Green, J. S. A. (1977). The Weather During July 1976: Some Dynamical Considerations of the Drought. *Weather*, *32*(4), 120–126. Retrieved 2023-04-19, from https://onlinelibrary.wiley.com/doi/abs/10.1002/j.1477-8696.1977.tb04532.x (_eprint: https://onlinelibrary.wiley.com/doi/pdf/10.1002/j.1477-8696.1977.tb04532.x) doi: 10.1002/j.1477-8696.1977.tb04532.x

Hartmann, D. L. (2015). *Global Physical Climatology: Second Edition* (2nd ed ed.). Kent: Elsevier Science & Technology. Retrieved 2023-04-16, from https://public.ebookcentral.proquest.com/choice/publicfullrecord.aspx?p=5754480 (OCLC: 1099348114)

Hasselmann, K. (1976). Stochastic climate models Part I. Theory. *Tellus*, *28*(6), 473–485. Retrieved 2023-04-19, from https://onlinelibrary.wiley.com/doi/abs/10.1111/j.2153-3490.1976.tb00696.x (_eprint: https://onlinelibrary.wiley.com/doi/pdf/10.1111/j.2153-3490.1976.tb00696.x) doi: 10.1111/j.2153-3490.1976.tb00696.x

Held, I. M. (1999, January). The macroturbulence of the troposphere. *Tellus A: Dynamic Meteorology and Oceanography*, *51*(1), 59–70. Retrieved 2023-04-19, from https://doi.org/10.3402/tellusa.v51i1.12306 (Publisher: Taylor & Francis _eprint: https://doi.org/10.3402/tellusa.v51i1.12306) doi: 10.3402/tellusa.v51i1.12306

Huang, C. S. Y., & Nakamura, N. (2016, January). Local Finite-Amplitude Wave Activity as a Diagnostic of Anomalous Weather Events. *Journal of the Atmospheric Sciences*, *73*(1), 211–229. Retrieved 2023-03-24, from https://journals.ametsoc.org/view/journals/atsc/73/1/jas-d-15-0194.1.xml (Publisher: American Meteorological Society Section: Journal of the Atmospheric Sciences) doi: 10.1175/JAS-D-15-0194.1

Huang, C. S. Y., & Nakamura, N. (2017). Local wave activity budgets of the wintertime Northern Hemisphere: Implication for the Pacific and Atlantic storm tracks. *Geophysical Research Letters*, *44*(11), 5673–5682. Retrieved 2023-03-31, from `https://onlinelibrary.wiley.com/doi/abs/10.1002/2017GL073760` (_eprint: https://onlinelibrary.wiley.com/doi/pdf/10.1002/2017GL073760) doi: 10.1002/2017GL073760

Kidson, J. W. (1991, September). Intraseasonal Variations in the Southern Hemisphere Circulation. *Journal of Climate*, *4*(9), 939–953. Retrieved 2023-04-16, from `https://journals.ametsoc.org/view/journals/clim/4/9/1520-0442_1991_004_0939_ivitsh_2_0_co_2.xml` (Publisher: American Meteorological Society Section: Journal of Climate) doi: 10.1175/1520-0442(1991)004⟨0939:IVITSH⟩2.0.CO;2

Kushner, P. J., & Held, I. M. (1998). A test, using atmospheric data, of a method for estimating oceanic eddy diffusivity. *Geophysical Research Letters*, *25*(22), 4213–4216. Retrieved 2023-04-19, from `https://onlinelibrary.wiley.com/doi/abs/10.1029/1998GL900142` (_eprint: https://onlinelibrary.wiley.com/doi/pdf/10.1029/1998GL900142) doi: 10.1029/1998GL900142

Leith, C. E. (1973, September). The Standard Error of Time-Average Estimates of Climatic Means. *Journal of Applied Meteorology and Climatology*, *12*(6), 1066–1069. Retrieved 2023-04-19, from `https://journals.ametsoc.org/view/journals/apme/12/6/1520-0450_1973_012_1066_tseota_2_0_co_2.xml` (Publisher: American Meteorological Society Section: Journal of Applied Meteorology and Climatology) doi: 10.1175/1520-0450(1973)012⟨1066:TSEOTA⟩2.0.CO;2

Lorenz, D. J., & Hartmann, D. L. (2001, November). Eddy–Zonal Flow Feedback in the Southern Hemisphere. *Journal of the Atmospheric Sciences*, *58*(21), 3312–3327. Retrieved 2023-03-31, from `https://journals.ametsoc.org/view/journals/atsc/58/21/1520-0469_2001_058_3312_ezffit_2.0.co_2.xml` (Publisher: American Meteorological Society Section: Journal of the Atmospheric Sciences) doi: 10.1175/1520-0469(2001)058⟨3312:EZFFIT⟩2.0.CO;2

Nakamura, H., & Shimpo, A. (2004, May). Seasonal Variations in the Southern Hemisphere Storm Tracks and Jet Streams as Revealed in a Reanalysis Dataset. *Journal of Climate*, *17*(9), 1828–1844. Retrieved 2023-04-16, from `https://journals.ametsoc.org/view/journals/clim/17/9/1520-0442_2004_017_1828_svitsh_2.0.co_2.xml` (Publisher: American Meteorological Society Section: Journal of Climate) doi: 10.1175/1520-0442(2004)017⟨1828:SVITSH⟩2.0.CO;2

Nakamura, N., & Zhu, D. (2010, September). Finite-Amplitude Wave Activity and Diffusive Flux of Potential Vorticity in Eddy–Mean Flow Interaction. *Journal of the Atmospheric Sciences*, *67*(9), 2701–2716. Retrieved 2023-03-24, from `https://journals.ametsoc.org/view/journals/atsc/67/9/2010jas3432.1.xml` (Publisher: American Meteorological Society Section: Journal of the Atmospheric Sciences) doi: 10.1175/2010JAS3432.1

Swanson, K. L., & Pierrehumbert, R. T. (1997, June). Lower-Tropospheric Heat Transport in the Pacific Storm Track. *Journal of the Atmospheric Sciences*, *54*(11), 1533–1543. Retrieved 2023-04-19, from `https://journals.ametsoc.org/view/journals/atsc/54/11/1520-0469_1997_054_1533_lthtit_2.0.co_2.xml` (Publisher: American Meteorological Society Section: Journal of the Atmospheric Sciences) doi: 10.1175/1520-0469(1997)054⟨1533:LTHTIT⟩2.0.CO;2

Thompson, D. W. J., & Barnes, E. A. (2014, February). Periodic Variability in the Large-Scale Southern Hemisphere Atmospheric Circulation. *Science*, *343*(6171), 641–645. Retrieved 2023-03-24, from `https://www.science.org/doi/10.1126/science.1247660` (Publisher: American Association for the

Advancement of Science) doi: 10.1126/science.1247660

Thompson, D. W. J., Crow, B. R., & Barnes, E. A. (2017, March). Intraseasonal Periodicity in the Southern Hemisphere Circulation on Regional Spatial Scales. *Journal of the Atmospheric Sciences*, *74*(3), 865–877. Retrieved 2023-03-31, from https://journals.ametsoc.org/view/journals/atsc/74/3/jas-d-16-0094.1.xml (Publisher: American Meteorological Society Section: Journal of the Atmospheric Sciences) doi: 10.1175/JAS-D-16-0094.1

Thompson, D. W. J., & Woodworth, J. D. (2014, April). Barotropic and Baroclinic Annular Variability in the Southern Hemisphere. *Journal of the Atmospheric Sciences*, *71*(4), 1480–1493. Retrieved 2023-03-31, from https://journals.ametsoc.org/view/journals/atsc/71/4/jas-d-13-0185.1.xml (Publisher: American Meteorological Society Section: Journal of the Atmospheric Sciences) doi: 10.1175/JAS-D-13-0185.1

Trenberth, K. E. (1981). Seasonal variations in global sea level pressure and the total mass of the atmosphere. *Journal of Geophysical Research: Oceans*, *86*(C6), 5238–5246. Retrieved 2023-04-16, from https://onlinelibrary.wiley.com/doi/abs/10.1029/JC086iC06p05238 (_eprint: https://onlinelibrary.wiley.com/doi/pdf/10.1029/JC086iC06p05238) doi: 10.1029/JC086iC06p05238

Trenberth, K. E. (1991, October). Storm Tracks in the Southern Hemisphere. *Journal of the Atmospheric Sciences*, *48*(19), 2159–2178. Retrieved 2023-04-16, from https://journals.ametsoc.org/view/journals/atsc/48/19/1520-0469_1991_048_2159_stitsh_2_0_co_2.xml (Publisher: American Meteorological Society Section: Journal of the Atmospheric Sciences) doi: 10.1175/1520-0469(1991)048⟨2159:STITSH⟩2.0.CO;2

Vitart, F., Ardilouze, C., Bonet, A., Brookshaw, A., Chen, M., Codorean, C., … Zhang, L. (2017, January). The Subseasonal to Seasonal (S2S) Prediction Project Database. *Bulletin of the American Meteorological Society*, *98*(1), 163–173. Retrieved 2023-03-31, from https://journals.ametsoc.org/view/journals/bams/98/1/bams-d-16-0017.1.xml (Publisher: American Meteorological Society Section: Bulletin of the American Meteorological Society) doi: 10.1175/BAMS-D-16-0017.1

Wang, L., Lu, J., & Kuang, Z. (2018). A Robust Increase of the Intraseasonal Periodic Behavior of the Precipitation and Eddy Kinetic Energy in a Warming Climate. *Geophysical Research Letters*, *45*(15), 7790–7799. Retrieved 2023-03-24, from https://onlinelibrary.wiley.com/doi/abs/10.1029/2018GL078495 (_eprint: https://onlinelibrary.wiley.com/doi/pdf/10.1029/2018GL078495) doi: 10.1029/2018GL078495

Wang, L., & Nakamura, N. (2015). Covariation of finite-amplitude wave activity and the zonal mean flow in the midlatitude troposphere: 1. Theory and application to the Southern Hemisphere summer. *Geophysical Research Letters*, *42*(19), 8192–8200. Retrieved 2023-04-16, from https://onlinelibrary.wiley.com/doi/abs/10.1002/2015GL065830 (_eprint: https://onlinelibrary.wiley.com/doi/pdf/10.1002/2015GL065830) doi: 10.1002/2015GL065830

Wang, L., & Nakamura, N. (2016, December). Covariation of Finite-Amplitude Wave Activity and the Zonal-Mean Flow in the Midlatitude Troposphere. Part II: Eddy Forcing Spectra and the Periodic Behavior in the Southern Hemisphere Summer. *Journal of the Atmospheric Sciences*, *73*(12), 4731–4752. Retrieved 2023-04-22, from https://journals.ametsoc.org/view/journals/atsc/73/12/jas-d-16-0091.1.xml (Publisher: American Meteorological Society Section: Journal of the Atmospheric Sciences) doi: 10.1175/JAS-D-16-0091.1

Xue, D., Lu, J., Qian, Y., & Zhang, Y. (2021). Evidence for Coupling Between the Subseasonal Oscillations in the Southern Hemisphere Midlatitude Ocean and Atmosphere. *Journal of Geophysical Research: Atmospheres*, *126*(4), e2020JD033872. Retrieved 2023-03-31, from https://onlinelibrary.wiley.com/doi/abs/10.1029/2020JD033872 (_eprint: https://onlinelibrary.wiley.com/doi/pdf/10.1029/2020JD033872) doi: 10.1029/2020JD033872

Supporting Information for "Regional Features of the 20-30 Day Periodic Behavior in the Southern Hemisphere Circulation"

Zhaoyu Liu[1], Lei Wang[1]

[1]Department of Earth, Atmospheric, and Planetary Sciences, Purdue University

Contents

QGPV-based local finite-amplitude activity

As mentioned in the main text, another way to calculate the local finite-amplitude wave activity is based on quasi-geostrophic potential vorticity (QGPV), given the fact that QGPV is a material conserved quantity. Following Huang and Nakamura (2016), the equation for QGPV based local finite-amplitude is showed below:

$$A_q(\phi_e, \lambda, z, t) = \frac{a}{cos\phi_e}(\int_{q'\geq 0, \phi\leq\phi_e, \lambda=const} q' cos\phi d\phi - \int_{q'\leq 0, \phi\geq\phi_e, \lambda=const} q' cos\phi d\phi), \quad (1)$$

where a is the earth radius, ϕ, λ, represents the latitude and longitude respectively, z is the pressure pseudoheight defined by $z = -Hln(p/1000hPa)$ with $H = 7km$, the QGPV $q(\phi, \lambda, z, t) = f + \zeta + \frac{f}{\rho_0}\frac{\partial}{\partial z}[\frac{\rho_0(\theta-\widetilde{\theta})}{\partial\widetilde{\theta}/\partial z}]$, in which $f = 2\Omega sin\phi$ is the Coriolis parameter, ζ is relative vorticity, θ is the potential temperature ($\widetilde{\theta}$ is the hemispheric averaged basic state), and $q' = q - Q(\phi_e)$ denotes the deviation from the reference QGPV at the equivalent latitudes. A monotonic relationship between ϕ_e and Q lies below:

$$\phi_e(Q) = arcsin[1 - \frac{S(Q)}{2\pi a^2}], \tag{2}$$

where $S(Q)$ is the area bounded by the Q contour. Additionally, to consider the LWA at all pseudo-height levels, the density weighted LWA along the whole column is defined following Wang and Nakamura (2015):

$$\langle A_q \rangle = \int_0^\infty e^{-z/H} A(\phi_e, \lambda, z, t) dz \Big/ \int_0^\infty e^{-z/H} dz. \tag{3}$$

References

Huang, C. S. Y., & Nakamura, N. (2016, January). Local Finite-Amplitude Wave Activity as a Diagnostic of Anomalous Weather Events. *Journal of the Atmospheric Sciences*, *73*(1), 211–229. Retrieved 2023-03-24, from `https://journals.ametsoc.org/view/journals/atsc/73/1/jas-d-15-0194.1.xml` (Publisher: American Meteorological Society Section: Journal of the Atmospheric Sciences) doi: 10.1175/JAS-D-15-0194.1

Wang, L., & Nakamura, N. (2015). Covariation of finite-amplitude wave activity and the zonal mean flow in the midlatitude troposphere: 1. Theory and application to the Southern Hemisphere summer. *Geophysical Research Letters*, *42*(19), 8192–8200. Retrieved 2023-04-16, from `https://onlinelibrary.wiley.com/doi/abs/10.1002/2015GL065830` (_eprint: https://onlinelibrary.wiley.com/doi/pdf/10.1002/2015GL065830) doi: 10.1002/2015GL065830

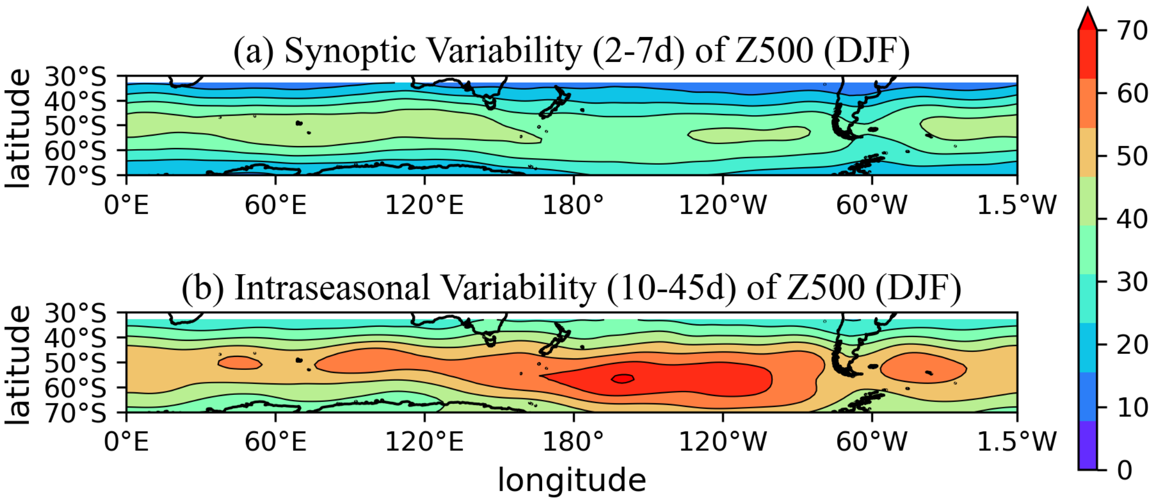

Figure S1. Bandpass-filtered variance converted to standard deviation for 500hPa geopotential height in austral summer(DJF): (a)synoptic variability(2-7 days), and (b)intraseasonal variability(10-45 days). The shading represents values between 0gpm and 70gpm.

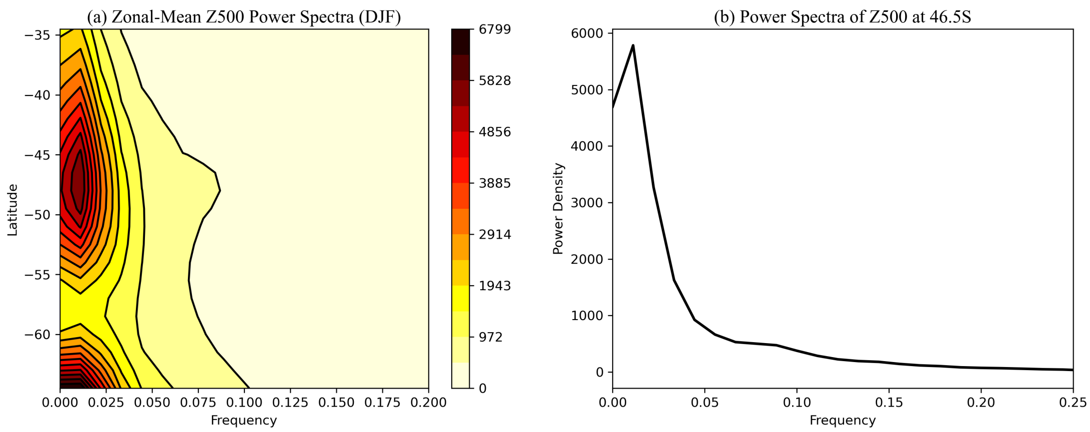

Figure S2. Power spectra in austral summer(DJF) of (a)zonal-mean Z500, and (b)zonal-mean Z500 at 46.5°S.

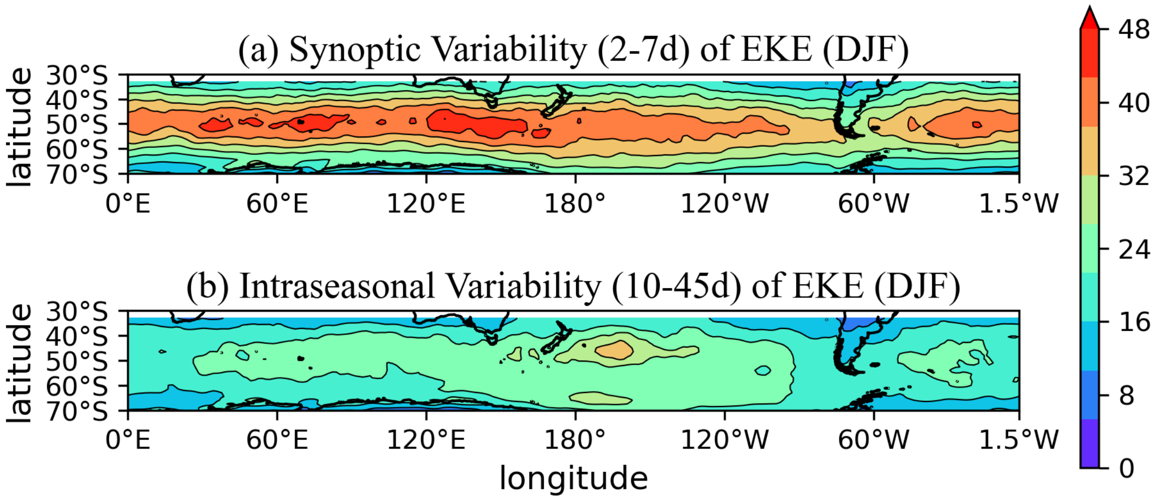

Figure S3. Bandpass-filtered variance converted to standard deviation for vertical averaged eddy kinetic energy (EKE) in austral summer(DJF): (a)synoptic variability(2-7 days), and (b)intraseasonal variability(10-45 days). The shading represents values between $0m^2/s^2$ and $48m^2/s^2$.

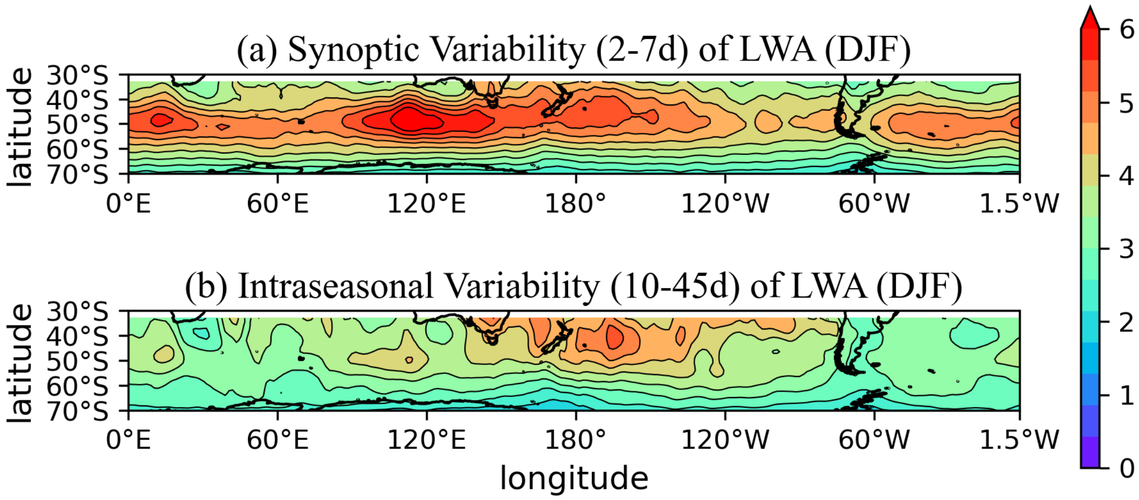

Figure S4. Bandpass-filtered variance converted to standard deviation for QGPV-based local wave activity in austral summer(DJF): (a)synoptic variability(2-7 days), and (b)intraseasonal variability(10-45 days). The shading represents values between $0m/s$ and $6m/s$.

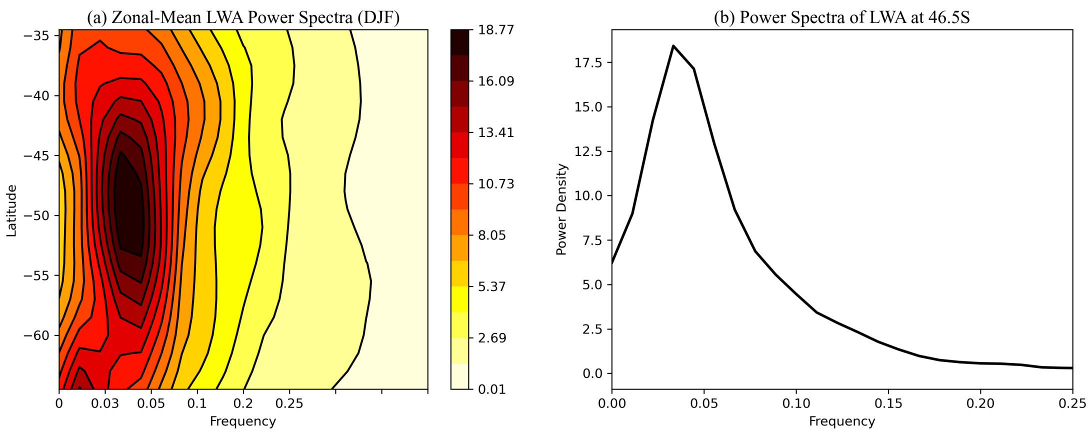

Figure S5. Power spectra in austral summer(DJF) of (a)zonal-mean QGPV-based LWA, and (b)zonal-mean QGPV-based LWA at 46.5°S.

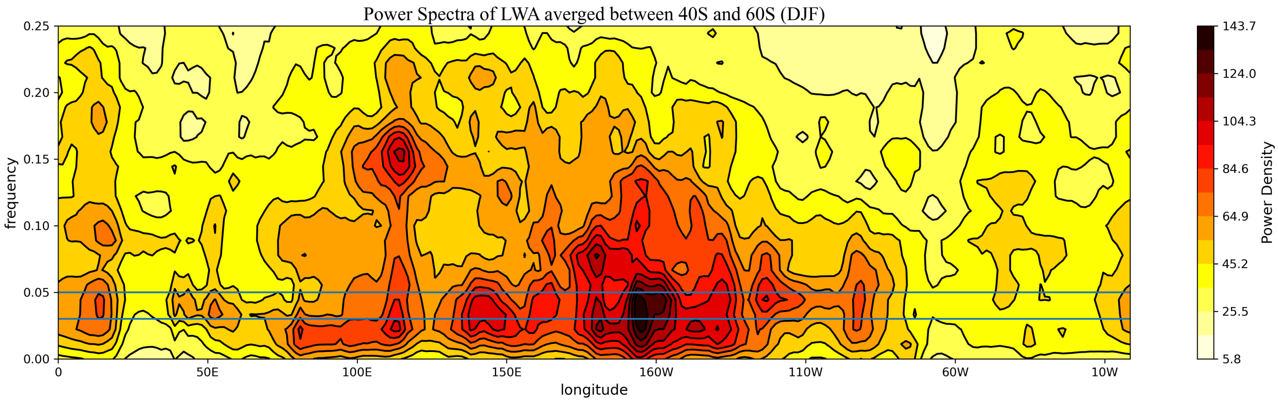

Figure S6. Power spectra of QGPV-based LWA averged between 40°S and 60°S as functions of longitude and frequency.

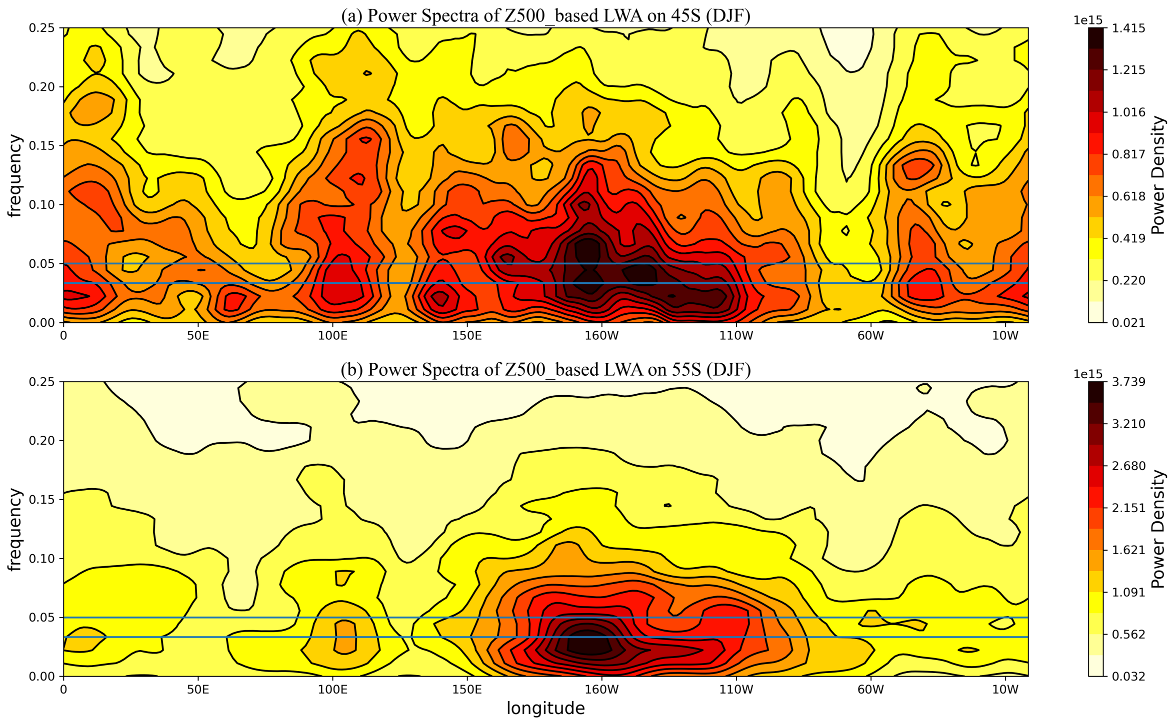

Figure S7. Power spectra of Z500-based LWA as functions of longitude and frequency at two representative latitudes 45°S (upper panel) and 55°S (lower panel), respectively.

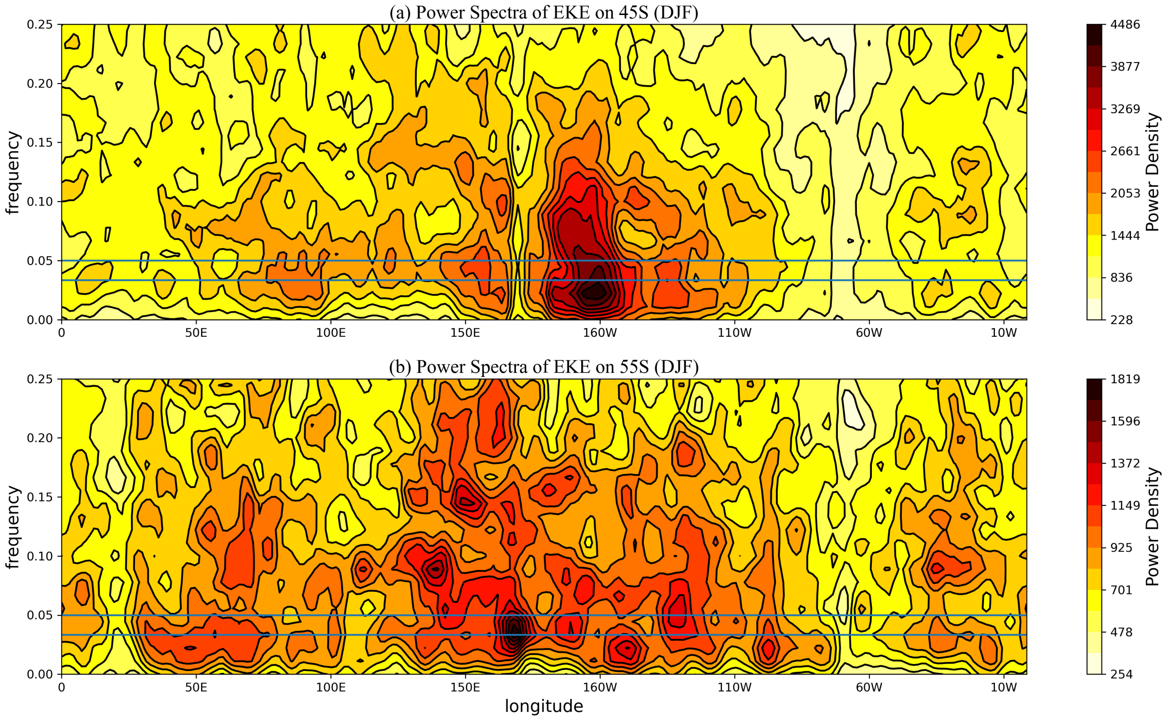

Figure S8. Power spectra of vertical averaged EKE as functions of longitude and frequency at two representative latitudes 45°S (upper panel) and 55°S (lower panel), respectively.

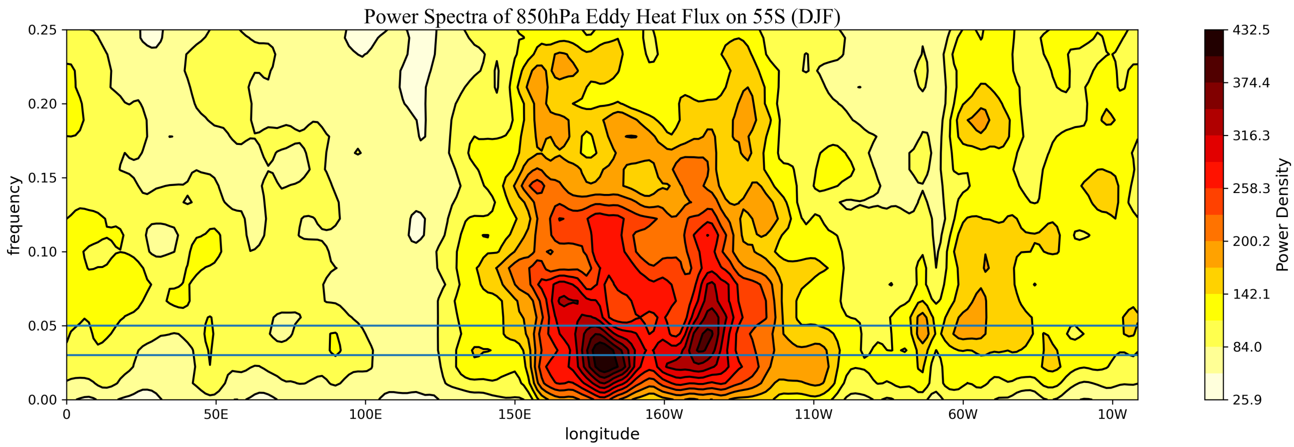

Figure S9. Power spectra of 850hPa eddy heat flux as functions of longitude and frequency at 55°S.